To the Graduate Council:

I am submitting herewith a dissertation written by Andrei Borisovich Oparin entitled "Extension of LSMS Techniques and Their Applications to Magnetic Multilayered Systems". I have examined the final copy of this dissertation for form and content and recommend that it be accepted in partial fulfillment of the requirements for the degree of Doctor of Philosophy, with a major in Physics.

Geoffrey S. Canright, Major Professor

We have read this dissertation
and recommend its acceptance:

Accepted for the Council:

Associate Vice Chancellor and
Dean of The Graduate School

EXTENSION OF LSMS TECHNIQUES AND THEIR APPLICATIONS TO MAGNETIC MULTILAYERED SYSTEMS

A Dissertation submitted for the Degree of **Doctor of Philosophy**

The University of Tennessee, Knoxville

Andrei Borisovich Oparin

May 2000

DEDICATION

This thesis is dedicated to my parents

Mr. Boris Alexeyevich Oparin

and

Mrs. Levtina Kapitonovna Oparin

who have given me invaluable educational opportunities.

ACKNOWLEDGEMENTS

I would like to thank Dr. Don M. N. Nicholson of ORNL for his supervision of the present project. His deep understanding of the physics involved made it possible to solve quite a few problems. I would like to thank my co-supervisor Dr. G. Malcolm Stocks of ORNL for his mentorship and partial support during my three and half year research at ORNL. The computational means that he put at my disposal were appreciated. A special thanks goes to Prof. Geoffrey S. Canright of the University of Tennessee, Knoxville for serving as my major Professor.

There are many more people to whom I am greatly indebted for the fruitful discussions that were helpful in completing this thesis. My thanks to Dr. Yang Wang, Dr. William A. Butler and Dr. X.-G. Zhang.

I thank Prof. Leo L. Riedinger for his continuous support as Dean of the Department of Physics and Astronomy at the University of Tennessee, Knoxville.

Special thanks to Alexander Babansky for his invaluable help with graphics.

A final thanks goes to all my friends and family.

ABSTRACT

In this thesis we pursued two goals, first, to improve the performance of the locally self-consistent multiple scattering, LSMS, method and second, to apply the method to a system of scientific interest.

The first goal was accomplished by placing an effective medium beyond the range of atoms usually used to calculate the charge density in the LSMS and by optimizing the speed of the matrix inversion.

The second goal was reached by performing first-principles local spin density calculations for models of interdiffused Cu/Py multilayers. Multiple, metastable, noncollinear magnetic structures that showed a reduced contribution to the saturation magnetization consistent with roughly one "magnetic dead" layer at the interface were found. The net magnetization obtained by averaging the calculated metastable magnetic configurations gave the total magnetization as a function of the permalloy layer thickness in good agreement with the experiment.

TABLE OF CONTENS

LIST OF FIGURES

Chapter 1

Introduction

For decades, density functional theory (DFT) of Hohenberg and Kohn [1] has been used in numerous methods to study electronic properties of many-electron systems. These authors proved that all features of the electronic structure of a system in a nondegenerate ground state are completely determined by its electron density. According to the theory, the total energy of a system is a unique functional of the electron density, and the correct density distribution minimizes this functional. Starting from the energy variational principle of DFT, Kohn and Sham [2] developed the local density approximation (LDA) to DFT. They proposed an approximate expression for the energy functional, which contains an expression for the exchange and correlation energy density at a point $\mathbf{r}$, that depends only on the electron density at $\mathbf{r}$. The local density approximation to density functional theory (DFT-LDA) produces a system of self-consistent one-particle Schrödinger equations with each electron moving in an effective potential consisting of the electrostatic and exchange-correlation potentials arising from the total electron density.

In order to calculate the physical properties of materials a number of band structure techniques have been developed. These techniques require only the atomic numbers and positions of the atoms in a crystal. They are referred to as first-principles (*ab initio*) methods. Several of them are based on the use of multiple-scattering

theory (MST) to solve the one electron Schrödinger equation. MST was introduced originally by Lord Rayleigh [3] in 1892. It provides a general approach to electronic structure calculations in solids. We note that MST has numerous advantages: 1) in principle, it leads to the exact answer; 2) it can be applied to systems with strong scattering such as transition metals; 3) taking advantage of the Green's function technique, it can be used to calculate physical properties of the solid directly from the Green's function; 4) it is readily implemented for the Dirac equation to treat the relativistic limit; 5) it does not require periodic boundary conditions so that a wide range of systems can be treated. The one shortcoming of MST seems to be in the somewhat more difficult implementation for potentials of general shape.

An object of primary interest in multiple-scattering theory is the scattering path operator $\boldsymbol{\tau}$. It carries information about all scattering processes within the solid. Theoretically, the matrix elements of the scattering path operator can be found by inverting a matrix, which is infinite in both the $\mathbf{R}_n$ and $L \equiv l, m$, where $\mathbf{R}_n$ is a set of lattice vectors and L is a combination of the angular and azimuthal quantum numbers l, m. For periodic systems, $\boldsymbol{\tau}$ can be recast in a form that is infinite only in L. In practice, the angular momentum index L is truncated at some maximum value l_{max}. In MST, potential dependent quantities are separated from those that depend on the geometry of the solid. This separation is very convenient since the structural quantities can be calculated just once for a given geometry.

In MST the total potential is considered to be the sum of the individual poten-

tials making up a system. The potential of each atom is defined to be zero outside the unit cell corresponding to that atom. There are no restrictions on the shape of the individual potentials. However, it is easier to implement MST when the potentials are of spherical symmetry and do not overlap. The so-called muffin-tin (MT) approximation method divides atomic cells into two regions: MT and interstitial. Inside the MT region, the effective potential possesses spherical symmetry, while outside the MT sphere, interstitial region, the potential is assumed to be constant. For this kind of potential, the multiple-scattering equations can be solved essentially exactly. Some researchers make use of a second spherical approximation technique in MST calculations. In this method, known as the atomic sphere approximation (ASA), the space is approximated by a collection of spheres centered at the nuclei, whose volume equals to the volume of the corresponding atomic cell. The multiple-scattering equations are only approximately correct for overlapping potentials.

MST has been applied to a wide variety of systems. Application of the MST to the electronic structure in periodic solids by Korringa [4] and later on by Kohn and Rostoker [5] has led to the KKR band theory method.

The Green's function approach to MST makes it possible to determine observables of the solid such as the electronic charge density and the density of states (DOS) if the Green's function is known. The analytic properties of the Green's function allow the energy integrals to be evaluated on a contour in the upper half of complex plane. Since the Green's function demonstrates smooth behavior far from

the real axis, the numerical evaluation of these integrals takes less computational effort.

In another step, the KKR was combined with the coherent potential approximation (CPA) [6] method resulting in the KKR-CPA method [7, 8, 9]. The KKR-CPA has proved to be a very helpful technique for calculating the electronic properties in substitutionally disordered alloys [10]. The theoretical boundaries are that, as a single-site theory, the KKR-CPA does not address short range order (SRO) and charge transfer effects. After studying some of these problems certain improvements have been made [11, 12]. Usually, the KKR-CPA assumes an isomorphous model of an alloy, in which all of the A and B atoms have the same potentials $v_A(\mathbf{r})$ and $v_B(\mathbf{r})$, respectively.

There are numerous problems of great importance that call for calculations in very large unit cells (supercells) where the number of atoms, N, in the supercell is of the order of several hundreds and more. In conventional LDA, the time required to carry out electronic structure calculations diverges as N^3. Even making use of powerful computers, LDA calculations in such systems were not realistic. Taking adventage of massively parallel processing (MPP) computers and the development of order-N methods, LDA calculations for large and complex systems became affordable. As follows from its definition, an order-N method is one, in which the computational effort increases linearly with N.

The locally self-consistent multiple scattering (LSMS) [13, 14] technique was

developed to study extended and complex systems. It displays order-N scaling in the solution of the equations of real space MST on unit cells with periodic boundary conditions. The problem of solving the LDA equations for an N-atom system is made tractable by decomposing into N linked locally self-consistent subproblems.

The central point of LSMS technique is based on the observation that a good approximation to the electron density and the density of states (DOS) on a particular atom within a large condensed system, and thereby the total energy of that system, can be obtained by considering only the electronic multiple scattering processes in a finite spatial region centered at that atom. The cluster of M atoms included in the region is referred to as the local interaction zone (LIZ) of the atom. Outside the LIZ, the multiple scattering equations are solved approximately, although the long range Coulomb interactions are taken into account exactly. Every atom in the system is considered to be at the center of its own LIZ. This fact can be used to obtain an approximation to the electron density and DOS, associated with every atom in the system. The algorithm is specifically designed for application to MPP architectures and to networks of computing resources using virtual parallelism packages such as Parallel Virtual Machines (PVM). Using this method, detailed study of electronic and magnetic behavior of alloys has been conducted and excellent agreement with experiment has been reported in the literature [15, 16].

Recently Abrikosov *et al* [17, 18] have proposed some extentions to improve the LSMS method. They developed the locally self-consistent Green's function method.

In this thesis, we come forward with a different extention, namely, the block diagonal approach, BDA.

There is a growing realization of the importance of understanding the magnetic behavior of systems in which the magnetic order is noncollinear [19, 20]. By noncollinear we mean that the magnetic moments associated with individual sites in the crystal are not aligned along the same axis of spin quantization. This is in contradistinction to the simple cases of ferromagnetic order, in which moments are parallel, anti-ferromagnetic order, in which different site moments align anti-parallel. Noncollinear magnetism occurs even in ordered systems with no chemical disorder such as Cr [21] and $MnAu_2$ [22, 23] which exhibit heliomagnetism. In disordered systems such as substitutionally disordered and amorhphous alloys noncollinear magnetism is more common [19, 24, 25, 26]. In addition, noncollinear magnetism is a feature of most magnetic system at finite temperature. Fortunately, MST provides a natural language for describing the electronic states of such spin canted systems. The locally self-consistent multiple scattering (LSMS) method can be extended to treat noncollinear magnetic systems. For example, the LSMS has been used to calculate the magnetic structure of a substitutionally disordered fcc $Fe_{65}Ni_{35}$ alloy that indicates the existence of a noncollinear ground state [27].

The above-mentioned extension of the LSMS technique can help us understand the magnetic structure of the interfaces in magnetic multilayers. An accurate representation of the magnetic structure at interfaces can lead to a much better un-

derstanding of giant magnetoresistance (GMR) effect in these systems. There are experiments [28, 29, 30, 31] and calculations [32] aimed at elucidating the magnetic structure of magnetic multilayers.

For some time, the moment as a function of the total amount of magnetic material deposited in Cu/Permalloy/Cu and Cu/Ni/Cu sandwiches, as well as Ni/Cu and Permalloy/Cu and other spin valves, has been measured, and the moment found to be less than expected from the amount of Ni and Fe deposited. In particular, for nickel thicknesses less than T_{nf} (thickness nonferromagnetic) no moment was observed, but with a further increase in thickness, the moment increased linearly with a slope given by the bulk magnetization of pure Ni. This showed that a nonmagnetic region is formed at the interface, and that away from the interface relatively undisturbed ferromagnetic material is present.

The magnetically soft ($Ni_{0.8}Fe_{0.2}$) solid solution known as permalloy, Py, is an extremely important alloy for magnetic device applications because of its extremely high permeability, its extremely low magnetostriction, and its high anisotropic magnetoresistance. It has another interesting attribute that may be important for applications, namely, it is an extremely good conductor for majority electrons and an extremely poor one for minority electrons. Py is a leading candidate for the ferromagnetic material in spin valves that have possible application in magnetic read heads, magnetic sensors and nonvolatile magnetic memory. The magnetic moments in Py are collinear [33], however, there are noncollinear moments near an interface

between Py and Cu [34].

We have used calculations to demonstrate that diffusion at the interface between Py and Cu results in noncollinear moments [34]. In our calculations multiple metastable magnetic configurations were found. The agreement between measured and calculated magnetization for the limited set of solutions obtained gives rise to a conclusion that the canting of the Fe moments and a reduction of the magnitude of the Ni moments at the interface is responsible for the measured "magnetically dead" layers. We also found that placing a small amount of Co at the interface dramatically increased the collinearity [35].

Chapter 2

Density Functional Theory

In their original paper, Hohenberg and Kohn [1] derived two important theorems. The first one is that the electron density $\rho(\mathbf{r})$ is uniquely determined by the external potential. By showing that two different external potentials could not lead to the same charge density, they proved that the reverse is also true, namely that the external potential is a unique functional of the charge density $\rho(\mathbf{r})$. Since the ground state wave function is determined by the external potential, it is also a unique functional of the charge density, and so is the ground state energy. The second theorem is that the energy functional assumes its minimum value, the ground state energy, for the correct ground state density.

2.1 Local Spin Density Approximation

Though exact in principle, the theory as it stands does not bring us any closer to a solution of the problem of finding the ground state energy or electron density, as all the information associated with the many-electron problem is contained in the unknown energy functional. Kohn and Sham [2] developed a method for the treatment of a system of strongly interacting electrons in the presence of nuclei. Their assumption was that the exchange-correlation energy functional is purely local and the corrections to the exchange-correlation energy due to nearby inhomogeneities

in the electron density can be neglected. These assumptions lead to the derivation of a set of single-electron Schrödinger equations, the Kohn-Sham equations, with effective local potentials. This method is known as the local density approximation, LDA. The local spin density approximation, LSDA, is the commonly used extension of these equations to magnetic systems (see, for instance, Kohn and Vashishta [36]).

According to the LSDA, the total energy for a system consisting of an arbitrary number of electrons in magnetic fields $\mathbf{B}(\mathbf{r})$ is given by

$$E[\nu(\mathbf{r})] = T[\rho(\mathbf{r})] + U[\rho(\mathbf{r})] + E_{xc}[\nu(\mathbf{r})] - \int \mathbf{m}(\mathbf{r}) \cdot \mathbf{B}(\mathbf{r})\, d\mathbf{r}, \tag{1}$$

and satisfies

$$\frac{\delta E[\nu(\mathbf{r})]}{\delta \nu(\mathbf{r})} = 0, \tag{2}$$

with the kinetic energy

$$T = \sum_{i(occ)} \int_{\infty} \psi_i^*(\mathbf{r})) \left[-\nabla^2 \psi_i(\mathbf{r})\right] d\mathbf{r} \tag{3}$$

and

$$\nu(\mathbf{r}) = \{\rho(\mathbf{r}), \mathbf{m}(\mathbf{r})\}. \tag{4}$$

The Coulomb potential is

$$U = -2 \sum_n \int_{\infty} \frac{Z_n \rho(\mathbf{r})}{|\mathbf{r} - \mathbf{R}_n|}\, d\mathbf{r} + \int_{\infty}\int_{\infty} \frac{\rho(\mathbf{r})\rho(\mathbf{r}')}{|\mathbf{r} - \mathbf{r}'|}\, d\mathbf{r}\, d\mathbf{r}' + \sum_{m \neq n} \frac{Z_n Z_m}{|\mathbf{R}_n - \mathbf{R}_m|}, \tag{5}$$

and the electronic charge density $\rho(\mathbf{r})$ is defined as

$$\rho(\mathbf{r}) = \sum_{i(occ)} \psi_i^*(\mathbf{r})\, \psi_i(\mathbf{r}), \tag{6}$$

and the magnetization density $\mathbf{m}(\mathbf{r})$ is given by

$$\mathbf{m}(\mathbf{r}) = -\mu_B \sum_{i,j(occ)} \sigma_{ij} \psi_i^*(\mathbf{r}) \psi_j(\mathbf{r}). \tag{7}$$

Here μ_B is the Bohr magneton and σ is the Pauli spin matrix vector. The $\psi_i(\mathbf{r})$ are the solutions of effective single-electron Schrödinger equation. The sums in the last expressions go over all the occupied states (including states that differ with respect to spin orientation) of the system with $\mathcal{N}$, the total number of electrons constrained by the following condition

$$\mathcal{N} = \int \rho(\mathbf{r})\, d\mathbf{r}. \tag{8}$$

The effective exchange-correlation energy E_{xc} is given by the local spin density approximation (LSDA)

$$E_{xc}[\nu] \approx \int \rho(\mathbf{r})\, \epsilon_{xc}(\nu(\mathbf{r}))\, d\mathbf{r}, \tag{9}$$

where $\epsilon_{xc}(\nu(\mathbf{r}))$ is the exchange-correlation energy density in a homogeneous electron gas of density $\rho(\mathbf{r})$ and moment $\mathbf{m}(\mathbf{r})$. For simplicity, we restrict ourselves here to the case where both $\mathbf{m}(\mathbf{r})$ and $\mathbf{B}(\mathbf{r})$ have only one nonvanishing component, say $m_z(\mathbf{r}) \equiv m(\mathbf{r})$ and $B_z(\mathbf{r}) \equiv B(\mathbf{r})$. Taking the functional derivative (Eq. (2)) leads to the following single-electron Schrödinger (Kohn-Sham) equations

$$-\nabla^2 + V_{coul}(\mathbf{r}) + \mu_{xc}(\mathbf{r}) - \sigma\mu_B[B(\mathbf{r}) - B_{xc}(\mathbf{r})]\ \psi_{i\sigma}(\mathbf{r}) = \epsilon_{i\sigma}\ \psi_{i\sigma}(\mathbf{r}), \sigma = \pm 1 \tag{10}$$

where

$$V_{coul}(\mathbf{r}) = \frac{\delta U}{\delta \rho(\mathbf{r})}, \tag{11}$$

$$\mu_{xc}(\mathbf{r}) = \frac{\delta E_{xc}[\rho, m]}{\delta \rho(\mathbf{r})}, \tag{12}$$

$$B_{xc}(\mathbf{r}) = \frac{\delta E_{xc}[\rho, m]}{\delta m(\mathbf{r})}, \tag{13}$$

and

$$\rho(\mathbf{r}) = \sum_{\sigma} \rho_{\sigma}(\mathbf{r}), m(\mathbf{r}) = -\mu_B \left[\rho_{+1}(\mathbf{r}) - \rho_{-1}(\mathbf{r})\right] \tag{14}$$

$$\rho_{\sigma}(\mathbf{r}) = \sum_{i(occ)} |\psi_{i\sigma}(\mathbf{r})|^2 \tag{15}$$

and $\epsilon_{i\sigma}$'s are Lagrange parameters and are viewed as the single-electron energies.

The orbitals $\psi_{i\sigma}(\mathbf{r})$ used to construct the electron density in Eqs. (14) and (15) are determined by solving the Kohn-Sham equations Eq. (10). The solutions of the Kohn-Sham equations, in turn, depend on the electron density via the effective potentials in Eqs. (11)-(13). To solve for the potential and the charge density, these equations have to be iterated until the electron density generated by the potential is identical to that used to construct the potential. This procedure is called the self-consistent field (SCF) calculation. Self-consistent field calculations are crucial in the field of electronic structure calculations, and yield measurable quantities such as the elastic moduli, lattice constants and energies of formation.

Successful investigations of many types of materials as well as calculation of total energies and magnetic moments within a few percent of the experimental values have led to the general conviction that the DFT-LSDA is a quantitative theory capable of calculating total energies and magnetic moments accurately.

We use atomic units throughout this thesis. In atomic units, energy is measured in Rydbergs, length in Bohr radii, and mass in units of half the electron mass. The

effect of this choice of units is to make the replacement $\hbar^2/2m = 1$ and $e^2 = 2$.

2.2 Local Density Approximation for Noncollinear Spins

So far we have exploited mathematics of eigenfunctions and eigenvalues to describe systems under consideration. For sake of compactness, it would be more convenient for us to start using Green's functions. It involves integral equations and calculations of traces instead of summation.

An essential difference between noncollinear and collinear magnets is the absence in the noncollinear case of a natural spin quantization axis common for the whole crystal. Fortunately, close to the i-th atom it is possible to identify a volume, Ω_i, in which the average magnetic moment points in the same direction over times long compared to the inter-site hopping time [37]. Accordingly, a unit vector $(\mathbf{e}_i)$, that specifies the local moment orientation associated with the i-th site, is defined through

$$\mathbf{e}_i = \frac{\int_{\Omega_i} \mathbf{M}_i(\mathbf{r})\, d\mathbf{r}}{|\int_{\Omega_i} \mathbf{M}_i(\mathbf{r})\, d\mathbf{r}|}. \tag{16}$$

For the sake of being definite, Ω_i can be taken as either a muffin-tin or atomic (ASA) sphere. A general non-collinear local moment state is then specified by a set of local orientations, $\{\mathbf{e}_i\}$.

For non-collinear systems the Kohn-Sham equations take the form

$$\{[\nabla^2 + \epsilon]\hat{1} - \hat{V}_{eff}\}\hat{G}(\mathbf{r}, \mathbf{r}'; \epsilon) = \hat{1}\delta(\mathbf{r} - \mathbf{r}'), \tag{17}$$

$$\hat{\rho}(\mathbf{r}) = -\frac{1}{\pi}\int_{-\infty}^{\infty} d\epsilon\, \hat{G}(\mathbf{r}, \mathbf{r}; \epsilon) f(\epsilon - \mu), \tag{18}$$

$$\hat{V}_{eff} = \left[V_{ext} + e^2 \int d\mathbf{r}' \frac{\rho(\mathbf{r}')}{|\mathbf{r} - \mathbf{r}'|} + \frac{\delta E_{xc}}{\delta \rho(\mathbf{r})} \right] \hat{1} + \left[\mathbf{B}_{ext} + \frac{\delta E_{xc}}{\delta \mathbf{m}(\mathbf{r})} \right] \cdot \hat{\sigma}. \qquad (19)$$

In Eq. 18 $\hat{\rho}(\mathbf{r})$ is the density matrix from which the charge $\rho(\mathbf{r}) = \mathrm{Tr}\hat{\rho}(\mathbf{r})$ and magnetization $\mathbf{m}(\mathbf{r}) = \mathrm{Tr}\hat{\sigma}\hat{\rho}(\mathbf{r})$ can be readily calculated. In these equations $\hat{O}$ signifies a matrix in 2×2 spin space and 'Tr' denotes a trace over spin, $f(\epsilon - \mu)$ is the occupation function and $\mathbf{B}_{ext}$ is the external magnetic field. For a recent review of LSDA techniques as applied to non-collinear magnetic states see Sandratskii [38].

It is important to note, even in a muffin-tin (or ASA) model, where $\hat{\rho}(\mathbf{r})$ and $\hat{V}_{eff}$ can be decomposed into a sum of (spherically symmetric) single site contributions ($\hat{\rho}(\mathbf{r}) = \sum_i \hat{\rho}^i(\mathbf{r}) w_i(\mathbf{r})$ and $\hat{V}_{eff}(\mathbf{r}) = \sum_i \hat{v}^i(\mathbf{r}) w_i(\mathbf{r})$ where $w_i(\mathbf{r})$ is the truncation function [39] for the Voronoi polyhedron), that the site charge densities, $\hat{\rho}^i(\mathbf{r})$, and potentials, $\hat{v}^i(\mathbf{r})$, are, in general, off diagonal in spin-space when referenced to a single (global) frame of reference. In the local approximation the spatial variation in the magnetization direction does not influence the exchange-correlation potential at a given point in either a muffin-tin or atomic (ASA) sphere. So at any point we can determine the form of the potential in the local system of this point. For such a system it is convenient to choose rectangular coordinates with the z axis to the magnetization direction at the point. In this reference frame $\hat{\rho}(\mathbf{r})$ is diagonal on average and, therefore, one can employ the results of the theory of the ferromagnetic electron gas (for instance, see [40]) to determine the form of exchange-correlation potential in Eq. (19). Transformation of the site charge density and potential from the global coordinates system to the local one can be done by making use of a

unitary transformation

$$\hat{U}\hat{O}_g\hat{U}^\dagger = \hat{U}\begin{pmatrix} O^i_{g,11} & O^i_{g,12} \\ O^i_{g,21} & O^i_{g,22} \end{pmatrix}\hat{U}^\dagger = \begin{pmatrix} O^i_{l,\uparrow(\mathbf{r})} & 0 \\ 0 & O^i_{l,\downarrow(\mathbf{r})} \end{pmatrix} = \hat{O}_l, \tag{20}$$

in which $\hat{O}_l$ has only *up* ($O^i_\uparrow$) and *down* ($O^i_\downarrow$) components. Here, $\hat{O}_i$ can be any site dependent quantity and the subscripts g and l refer to global and local frames of reference. It is also useful to note that, for the single-site potential, Eq.(20) implies

$$\hat{v}^i = \frac{1}{2}(v^i_\uparrow + v^i_\downarrow)\hat{I} + \frac{1}{2}(v^i_\uparrow - v^i_\downarrow)\hat{\sigma}\cdot\mathbf{e}_i\,, \tag{21}$$

where $\mathbf{e}_i$ is the unit vector defined above in Eq. (16).

The problem of the self-consistent determination of the density matrix is usually solved within an iteration process employing one of the modern methods of solving the Kohn-Sham equation (17) with the effective potential (19). In the next section we give a very detailed description of one of such methods, namely, the LSMS technique [14].

Chapter 3

Multiple Scattering Theory

The multiple scattering theory (MST) has been used extensively in studying the electron behavior in solids. In the one-electron model, solids can be considered as an assembly of individual scatterers. Each scatterer is described by a local potential $v_i(\mathbf{r})$ which is determined according to the local density functional theory [1, 2]. Applications of MST to ordered and disordered solids lead to the Korringa-Kohn-Rostoker(KKR) band theory method [4, 5] and the KKR coherent potential approximation method [6, 41], respectively. Compared with other approaches, MST has proved to be the most elegant way to the electronic structure calculations. No restriction is imposed by the theory on the spatial arrangement of the constituent potentials. It is, however, much easier to implement the MST when the individual potentials are bounded by spheres that do not overlap. In this chapter, the MST is briefly reviewed.

3.1 Multiple-scattering equations

In the multiple scattering theory, the ensemble potential $V(\mathbf{r})$ is taken as the sum over non-overlapping potentials $v_i(\mathbf{r})$ centered at each site [10],

$$V(\mathbf{r}) = \sum_{i=1}^{N} v_i(\mathbf{r}_i), \tag{22}$$

where $v_i(\mathbf{r}_i)$ are assumed to be zero outside a bounding sphere of radius R. The Green's function for the crystal, valid for r' either inside or outside the bounding sphere, can be written as [42]

$$G(\mathbf{r},(\mathbf{r}');\epsilon) = \sum_{L,L'} Z_L^i(\mathbf{r},\epsilon)\,\tau_{LL'}^{ij}(\epsilon) Z_{L'}^j((\mathbf{r}'),\epsilon) - \sum_L Z_L^i(\mathbf{r},\epsilon) J_L^i((\mathbf{r}'),\epsilon), \qquad (23)$$

where the functions $Z_L^i(\mathbf{r},\epsilon)$ and $J_L^i(\mathbf{r},\epsilon)$ are regular and irregular solutions of the Schrödinger equation in the ith Wigner-Seitz cell. The superscripts on the elements of the scattering path operator $\tau_{LL'}^{ij}$ [43] refer to the cells centered at the lattice sites $\mathbf{R}_i$ and $\mathbf{R}_j$, and the subscripts are the angular momentum indices. The presence of of the variable ϵ explicitly indicates the energy dependence of the scattering path operator. The scattering path operator is obtained from the inverse of the matrix

$$\mathbf{M} = \mathbf{m} - \mathbf{g}, \qquad (24)$$

i.e., $\boldsymbol{\tau} = \boldsymbol{M}^{-1}$. The only non-zero elements of matrix $\mathbf{m}$ are diagonal blocks $\mathbf{m}^i$ corresponding to $i = j$. The matrix $\mathbf{m}$ is the inverse of the scattering t-matrix for the atom on site i. For spherically symmetric potentials, elements of $\mathbf{m}$ are given by

$$m_{LL'}^i = (-\kappa \cot\theta_l^i + i\kappa)\delta_{LL'}, \qquad (25)$$

where $\kappa = \sqrt{\epsilon}$. The phase shifts θ_l are energy dependent and contain all the scattering information. The elements of $\mathbf{g}$ are free electron propagators for s, which are defined in the real space as

$$g_{LL'}^{ij}(\epsilon) = -4\pi\kappa\, i^{l-l'+1} \sum_{L''} C_{LL'}^{L''}\, i^{-l''}\, h_{l''}^+(\kappa\,|\mathbf{R}_i - \mathbf{R}_j|)\, Y_{L''}(\mathbf{R}_i - \mathbf{R}_j)(1-\delta_{ij}). \qquad (26)$$

The matrix elements of diagonal blocks ($i = j$) are equal to zero. The $C_{LL'}^{L''}$ are the Gaunt factors given by

$$C_{LL'}^{L''} = \int Y_L(\Omega)\, Y_{L''}(\Omega)\, Y_{L'}(\Omega)\, d\Omega, \tag{27}$$

where Y_L and h_l^+ are the spherical harmonics and Hankel functions. The Gaunt factors are equal to zero unless $l + l' + l''$ is even, and they also vanish if $l'' > l' + l$ (recall that $L \equiv \{l, m\}$). It is conventional to truncate the angular momentum expansions at some l_{max}. If there are N atoms in the crystal, the dimensions of $\mathbf{M}$ are $N(l_{max}+1)^2 \times N(l_{max}+1)^2$. The matrix elements $\tau_{LL'}^{ij}$ are the ij, LL' elements of $\mathbf{M}^{-1}$. Once the Green's function is determined from Eq. (23), the charge density and the density of states are calculated from

$$\rho(\mathbf{r}) = -\frac{1}{\pi}\mathrm{Im} \int_{-\infty}^{\epsilon_F} G(\mathbf{r}, \mathbf{r}, \epsilon)\, d\epsilon, \tag{28}$$

and

$$\rho(\epsilon) = -\frac{1}{\pi}\mathrm{Im} \int_{\Omega_{ws}} G(\mathbf{r}, \mathbf{r}, \epsilon)\, d\mathbf{r}, \tag{29}$$

respectively. In the above equations, ϵ_F is the Fermi energy and Ω_{ws} is the volume of the Wigner-Seitz cell.

The electronic structure calculations based on the MST have been simplified considerably by using spherical potential approximations for the constituent potentials. The MT and the ASA methods have been very successful in predicting physical properties of many materials. Nevertheless, each approach has problems that limits its applications to certain systems. The long range Coulomb energy is

calculated with sufficient accuracy within the MT approximation, but the method runs into difficulties with large charge transfers in alloys. The reason is that the interstitial charges are averaged over all the cells in the system. As for the ASA, because of the overlap of the atomic spheres, the assumptions in the proof of the multiple-scattering equations are not valid. In the following section we discuss the MT energy functionals.

3.2 Muffin-tin approximation

In the muffin-tin approximation, described here for the case of one atom per unit cell, the electron charge density in each unit cell is replaced by its spherical average within the inscribed sphere of radius R_{mt} and by a constant charge density ρ_0 in the interstitial region,

$$\rho_i(\mathbf{r}) = \begin{cases} \rho_{mt}(r) & \text{if } r \leq R_{mt} \\ \rho_0 & \text{if } \mathbf{r} \in \Omega_{int} \end{cases} . \tag{30}$$

In the above expressions, the MT and interstitial quantities are represented by subscripts mt and int respectively. The charge neutrality requires

$$\rho_0 \Omega_{int} = Z - 4\pi \int_0^{R_{mt}} r^2 \rho(r)\, dr, \tag{31}$$

where the interstitial volume Ω_{int} is given by

$$\Omega_{int} = \Omega_{ws} - \frac{4\pi}{3} (R_{mt})^3. \tag{32}$$

The electron charge density is taken to be the same in each of the N unit cells of

the crystal, therefore, the potential energy term in Eq. (5) takes the following form

$$U = N\Big(-2\sum_n \int_{\Omega_{ws}} \frac{Z_n \rho(\mathbf{r})}{|\mathbf{r}-\mathbf{R}_n|}\, d\mathbf{r} + \sum_n \int_{\Omega_{ws}} \int_{\Omega_{ws}} \frac{\rho(\mathbf{r})\rho(\mathbf{r}')}{|\mathbf{r}-\mathbf{r}'-\mathbf{R}_n|} d\mathbf{r}\, d\mathbf{r}' + \\ + \sum_{m\neq n} \frac{Z_n Z_m}{|\mathbf{R}_n - \mathbf{R}_m|}\Big). \qquad (33)$$

The integrals over the Wigner-Seitz cell can be broken up into integrals over the MT spheres, within which the charge density is spherically symmetric, and integrals over the interstitial regions, where the charge density is constant. The Coulomb energy per unit cell can be expressed as

$$u[\rho] = -8\pi Z \int_0^{R_{mt}} r\rho(r)\, dr + 2(4\pi)^2 \int_0^{R_{mt}} dr\, r\rho(r) \int_0^{r} dr'\, r'^2\, \rho(r') - \frac{1}{2} C \frac{(\rho_0 \Omega_{int})^2}{a} \qquad (34)$$

In the last expression, a is the lattice constant, and C, which is different for each crystal lattice, is given by [44]

$$C = \frac{4\pi a^3}{\Omega_{int}^2}\left[\frac{\Omega_{ws}^2 A}{2\pi a^3} - \frac{6\Omega_{ws} + 4\Omega_{int}}{5}\left(\frac{R_{mt}}{a}\right)^2\right]. \qquad (35)$$

The constant A is expressed by

$$\frac{A}{a} = \frac{1}{\Omega_{ws}} \int \frac{d^3 r}{r} - \sum_n{}' \frac{1}{R_n}, \qquad (36)$$

and can be evaluated by the Ewald method [45]. The prime on the sum excludes the $\mathbf{R}_n = 0$ term.

The one-electron potential in each unit cell is expressed as

$$v(\mathbf{r}) = \begin{cases} v_{coul}(r) + v_{xc}(\rho_{mt}(r)) & \text{if } r \leq R_{mt} \\ v_0 + v_{xc}(\rho_0) & \text{if } \mathbf{r} \in \Omega_{int} \end{cases}, \qquad (37)$$

where, the potentials $v_{coul}(r)$ and v_0 are calculated by taking the functional derivative of the Coulomb energy per unit cell,

$$v_{coul}(r) = \frac{\delta u[\rho_{mt}, \rho_0]}{\delta \rho_{mt}(r)}, \tag{38}$$

and

$$v_0 = \frac{\delta u[\rho_{mt}, \rho_0]}{\delta \rho_0}. \tag{39}$$

The constant potential $v_0 + v_{xc}(\rho_0)$ is known as the MT zero, and the Fermi level is measured with respect to this quantity.

Using the local density scheme of Kohn and Sham, the exchange-correlation energy is of the form

$$E_{xc} = \int \rho(\mathbf{r}) \epsilon_{xc}(\rho)\, d\mathbf{r}, \tag{40}$$

and the kinetic energy term Eq. (3), is calculated from the following

$$T[\rho] = \sum_n \epsilon_n - \sum_i \int_{\Omega_i} v_i(\mathbf{r})\, \rho_i(\mathbf{r})\, d\mathbf{r}, \tag{41}$$

where $v(\mathbf{r})$ is the one-electron potential. The first term is the sum of the one-electron energies ϵ_n of the occupied states.

The local potentials and charge densities are determined from self-consistent field calculations. An initial guess for the local potential in the Schrödinger equation determines the one electron wave function $\psi_i(\mathbf{r})$, from which the local charge density is obtained. The charge density is then used to calculate a new potential. This iterative process continues until the difference between the new and the previous potential falls within the desired tolerance.

The MT approximation has been applied to many systems of interest and has given the total energy and elastic constants for transition metals [46] with reasonable accuracy.

3.3 The LSMS method

One derives the electric charge density in LSDA calculations from the single-electron Schrödinger equation Eq. (10). For almost all of the conventional methods, the CPU time required for matrix manipulation increases as $O(N^3)$ for a system of N atoms. The energy properties of a number of small systems have been treated with great precision using conventional techniques. Nevertheless, there are important classes of problems where it is necessary to treat the interactions between several hundred or even thousands of atoms. These classes include disordered and amorphous alloys, grain boundaries, surface and interface structures, and non-collinear magnetic structures in metals, alloys, layered systems and so on. It is obvious that even great accomplishments in the CPU speed can't handle the codes that scale like N^3 because it will still be too time consuming for some N. The locally self-consistent multiple-scattering (LSMS) method, in which $O(N)$ scaling is achieved using the parallel algorithm [47], was developed to treat these very large systems. It extends the standard reciprocal space band structure algorithm for solving the LSDA Schrödinger equations to unit cells consisting of hundreds or thousands of atoms, and is designed specifically for the implementation on massively parallel pro-

cessors (MPP). The parallel algorithm assigns a compute node to each site in the system to decompose the N-atom problem into N linked sub-problems. Based on the real space multiple-scattering theory, the LSMS uses the analytic properties of the single particle Green's function and the stationary properties of a LDA free energy functional [48], and approximates the electron density and the density of states (DOS) on each site by considering the scattering processes in a cluster of M atoms within a finite spatial region. The charge density for the entire system can be found for all sites in the system. Since calculations of the single-site quantities can be assigned to each node, and each node requires the inversion of a matrix of dimension $(l_{max}+1)^2 M$ the overall scaling is proportional to $M^3 N$.

The LSMS has been applied to the calculation of the total energy of disordered alloys, which resulted in the excellent agreement with experimental measurements. The extension of the LSMS method to treat noncollinear magnetic systems has given rise to some results for the magnetic structure of a substitutionally disordered fcc $Fe_{65}Ni_{35}$ alloy that indicates the existence of a noncollinear ground state [27]. Also, the above-mentioned extension has helped to find noncollinear moments near an interface between Py and Cu [34].

The LSMS algorithm and its implementation on the parallel supercomputers are discussed in the following subsections.

3.4 Algorithm

It is well-known that the quantity of interest in the LDA is the electronic charge density $\rho(\mathbf{r})$. By noting that the total energy is stationary with respect to variations in $\rho(\mathbf{r})$, LDA calculations for large systems are greatly simplified in the LSMS procedure. It leads to the possibility to make use of an approximation to the exact charge density without producing a large error in the total energy of the system.

The center point of the LSMS method is to consider the electronic multiple scattering processes only in a finite spatial region centered at each site. The cluster of M atoms included in the region is referred to as the local interaction zone (LIZ) of the atom. Within each LIZ, the Schrödinger equation (10) is solved to obtain the electronic charge density and the density of states (DOS) on the central atom. Outside the LIZ, the atoms are replaced by a constant background potential. Every atom in the system is taken to be at the center of its own LIZ. This fact is exploited in the LSMS to obtain an approximation to the electron density ρ_M^i and DOS $n_M^i(\epsilon)$ associated with every atom in the system ($i = 1, 2, \ldots, N$).

According to the above algorithm, the electronic structure problem can be reduced to that of calculating the single particle Green's function at the central site of a finite size cluster. For a LIZ of M atoms, the scattering path matrix $\boldsymbol{\tau}$ [43] in real space is given by

$$\boldsymbol{\tau}_M^s(\{\xi\}_i, \epsilon) = \left[(\mathbf{t}_M^s)^{-1}(\{\xi\}_i, \epsilon) - \mathbf{g}_M^s(i, \epsilon)\right]^{-1} \tag{42}$$

where the symbol $\{\xi\}_i$ denotes the configuration of atoms within the LIZ of atom

i, and ϵ is the single-electron energy parameter. The real space structure constant, $\mathbf{G}^s_M(i,\epsilon)$, is composed of a $M \times M$ array of free-particle propagator subblocks $\mathbf{g}^s_{jk}(\epsilon)$ that connects sites j and k. The t-matrix, $\mathbf{T}^s_M(\{\xi\}_i,\epsilon)$, has M non-zero subblocks on the diagonal, each of which corresponds to a single-site scattering matrix $\mathbf{t}^s_j$, where $j,k = 1,2,\ldots,M$. The spin-dependent electronic charge density on the ith atom can be found from the imaginary part of the one-electron Green's function (Eq. (23)) as follows

$$\rho^{s,i}_M(\mathbf{r}) = -\frac{1}{\pi}\,\mathrm{Im}\int_{-\infty}^{\infty} d\epsilon\, f(\epsilon-\mu)\left\{\sum_{LL'} Z^{s,i}_L(\mathbf{r},\epsilon)[\tau^s_M(\{\xi\}_i,\epsilon)]^{ii}_{LL'} Z^{s,i}_{L'}(\mathbf{r},\epsilon) - \right.$$
$$\left. - \sum_L Z^{s,i}_L(\mathbf{r},\epsilon) J^{s,i}_L(\mathbf{r},\epsilon)\right\}. \quad (43)$$

Everywhere above the symbol s stands for spin. Given the electron density for each spin channel, the magnetic spin moment, μ_i, can be calculated using

$$\mu_i = \int_{\Omega^i} d\mathbf{r}\{\rho^{\uparrow,i}_M(\mathbf{r}) - \rho^{\downarrow,i}_M(\mathbf{r})\}, \quad (44)$$

where Ω^i is the atomic cell volume of site i. Once the $\rho^{s,i}(\mathbf{r})$, the charge density associated with the site i is known, one can determine the total charge density $\rho(\mathbf{r})$ by adding up contributions from each site in the system,

$$\rho(\mathbf{r}) = \sum_{s,i} \rho^{s,i}(\mathbf{r}). \quad (45)$$

The LSDA one-electron potential to be used for the next SCF iteration is then reconstructed, which involves solving Poisson's equation, with an appropriate boundary condition on the large cell boundary, for a total electric density made up of a sum

of the single site densities. The ground state total energy is obtained from

$$E[\nu(\mathbf{r})] = \int_{-\infty}^{\infty} \epsilon n(\epsilon, v[\rho(\mathbf{r})])\, f(\epsilon - \mu)\, d\epsilon - \int \rho v[\rho(\mathbf{r})]\, d\mathbf{r} + U[\rho(\mathbf{r})] + E_{xc}[\nu(\mathbf{r})] - \\ - \int \mathbf{m}(\mathbf{r}) \cdot \mathbf{B}(\mathbf{r})\, d\mathbf{r}, \quad (46)$$

where $f(\epsilon - \mu)$ is Fermi function, μ the chemical potential determined from $\mathcal{N}$ the number of electrons in the system

$$\mathcal{N} = \int_{\infty} \rho(\mathbf{r}) d\mathbf{r}, \quad (47)$$

and $U[\rho(\mathbf{r})]$ and $E_{xc}[\nu(\mathbf{r})]$ are the Coulomb and exchange-correlation energies, $\nu(\mathbf{r})$ is defined previously in Eq. (4).

The above method is highly scalable on parallel supercomputers, since the task of calculating the $\boldsymbol{\tau}$-matrix, the electron density, and the DOS on each site can be assigned to a compute node. In calculating the matrix elements of $\boldsymbol{\tau}$, each node is required to invert a matrix of dimension $(l_{max}+1)^2 M$. Since M the number of atoms in the LIZ is independent of the system size N, the overall scaling is of order-N. Compared to the reciprocal space KKR method that inverts a matrix of dimension $(l_{max}+1)^2 \times N$ at a sufficient number of k-points to converge necessary BZ integrations, order-N scaling of the LSMS method is a clear advantage for $M \ll N$. It ought to be noted that the LSMS has the same range of applications as the KKR band theory method for the treatment of ordered solids.

3.5 Extension to Noncollinear Magnetic Systems

Assuming that the exchange field orientation is sufficiently constant over some volume surrounding each atomic site, it is possible to define for each atom a local, site dependent, frame of reference in which the local magnetic field aligns in the local "up" or "down" direction $\mathbf{e}$. In this local frame, conventional techniques for calculating the scattering matrix for a single site can be applied. Since each site has its own local frame, unitary transformations are necessary in order to construct the scattering path matrix required when calculating the Green's function. In the vicinity of site i, the Green's function is given by

$$\hat{\mathcal{G}}_M(\{\xi,\mathbf{e}\}_i,\mathbf{r},\epsilon)=\sum_{LL'}\hat{Z}^i_L(\mathbf{r},\epsilon)[\hat{\tau}_M(\{\xi,\mathbf{e}\}_i,\epsilon)]^{ii}_{LL'}\hat{Z}^i_{L'}(\mathbf{r},\epsilon)-\sum_L\hat{Z}^i_L(\mathbf{r},\epsilon)\hat{J}^i_L(\mathbf{r},\epsilon)\,, \quad (48)$$

where $\hat{\tau}_M(\{\xi,\mathbf{e}\}_i,\epsilon)$ is the scattering path matrix for a M-atom LIZ centered on atom i, ϵ is the one-electron energy parameter, and $\{\xi,\mathbf{e}\}_i$ represents a chemical and exchange field configuration of the LIZ. The functions, $\hat{Z}^i_L(\mathbf{r},\epsilon)$ and $\hat{J}^i_L(\mathbf{r},\epsilon)$, are regular and irregular solutions of the Schrödinger equation (17) for the local potential. Note that in the above expressions the Green's function is a 2×2 matrix in spin space (denoted by $\hat{}$) due to noncollinear magnetic interactions.

Given the Green's function in either the local or the global frame, the electron density and the magnetic moment density can be found by using

$$\rho^i(\mathbf{r})=-\frac{1}{\pi}\mathrm{Im}\,\mathrm{Tr}\left[\int_{-\infty}^{\infty}\hat{\mathcal{G}}_M(\{\xi,\mathbf{e}\}_i,\mathbf{r},\epsilon)\,f(\epsilon-\mu)\,d\epsilon\right] \quad (49)$$

and

$$\mathbf{m}^i(\mathbf{r}) = -\frac{1}{\pi}\mathrm{Im}\,\mathrm{Tr}\left[\int_{-\infty}^{\infty} \hat{\mathcal{G}}_M(\{\xi,\mathbf{e}\}_i,\mathbf{r},\epsilon)\hat{\sigma}\, f(\epsilon-\mu)\, d\epsilon\right], \tag{50}$$

where ϵ_f is the Fermi energy and each component of the vector $\hat{\sigma}$ correponds to a Pauli matrix. The new local exchange field orientation $\mathbf{e}^i$ for each site is determined by

$$\mathbf{e}^i = \int_{\Sigma^i} d\mathbf{r}\, \mathbf{m}^i(\mathbf{r}) \Big/ \left| \int_{\Sigma^i} d\mathbf{r}\, \mathbf{m}^i(\mathbf{r}) \right|. \tag{51}$$

As the LDA SCF iterations proceed, $\mathbf{e}^i$ will rotate in order to minimize the total energy. Thus we can visualize a noncollinear magnetic structure in which the orientations of the local moments vary from site to site. In calculating the matrix elements of $\boldsymbol{\tau}$, each node is required to invert a matrix of dimension $2(l_{max}+1)^2M$ twice as large compared to a collinear system.

3.6 Parallel implementation

The LSMS technique has been implemented on the Intel MP Paragon XP/S systems. The mapping of the LSMS algorithm onto a MPP platform for a one atom per node case is discussed next.

Let us consider the ith atom of an N-atom system. An initial guess for the potential and electron density at site i and the positions of all the atoms are fed to the ith node. Each node determines all the nodes within its own LIZ. It then calculates the t-matrix ($\boldsymbol{t}^i$) corresponding to the potential at site i. It receives the t-matrices from other nodes and sends its own t-matrix to the nodes for which it is one

of the atoms in the remote node's LIZ. The ith node now has sufficient information to calculate the real space $\boldsymbol{\tau}_M(\{\xi\}_i, \epsilon)$ matrix Eq. (42),and the $\rho_M^i(\mathbf{r})$ Eq. (43). After this procedure is executed by all the nodes, the total electron density can be determined from Eq. (45), and the potential for the next iteration can be constructed. This process is repeated to self-consistency. A schematic representation of the above procedure is provided in Fig. 1.

The convergence properties of the LSMS as a function of LIZ size are among the main topics of the next section.

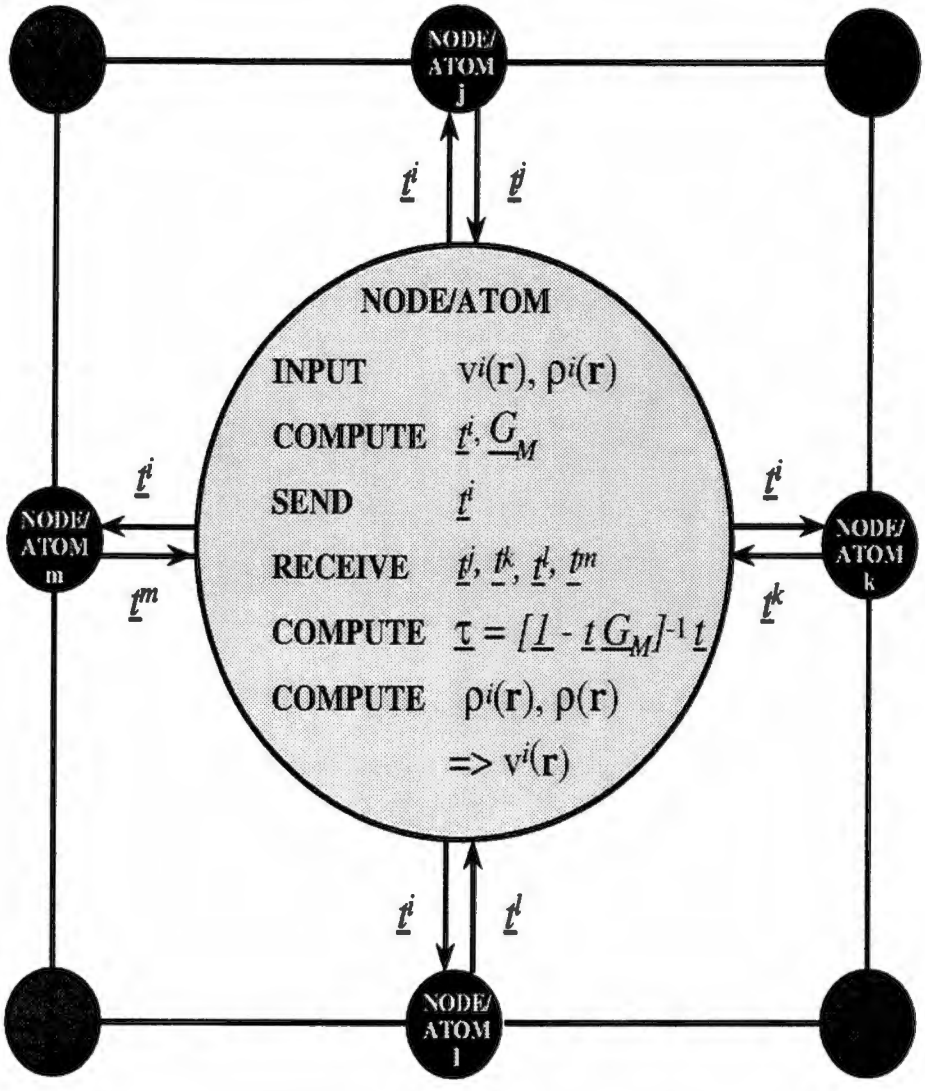

Figure 1: Schematic of a parallel SCF algorithm.

Chapter 4

Energy Convergence of LSDA Calculations using the Locally Self-consistent Multiple Scattering Method

In the study of solid solutions, amorphous metals, defected crystals, and other complex structures it is often useful to perform first principles local density calculations of the same sort that are routinely carried out for small unit cell ordered crystals. However, for complex structures hundreds or thousands of atoms will be required to adequately represent the structure. Unfortunately, the number of operations required by standard techniques increases as the third power of the number of atoms, N. This problem is overcome by the locally self-consistent multiple scatering method, LSMS, which can solve the Kohn-Sham equations associated with a cell, containing N atoms in a number of operations that grows linearly with N. This is accomplished by using multiple scattering theory to calculate the charge density on each particular atom with the approximation that there is no scattering from atoms outside a limited set of surrounding atoms. The set is referred to as the local interaction zone, LIZ of the atom. The potential is taken to be constant beyond the LIZ. The critical parameter that determines the accuracy of the solution is the number of atoms, M, in the LIZ. For many applications, M can be as small as a few

tens of atoms, for others a few hundred may be required. Because the number of operations increases as M^3 it is desirable to keep M small.

One way to accelerate convergence in M is to replace the constant potential beyond the LIZ with a medium that provides a more realistic description of the scattering from the remainder of the system. The locally self-consistent Green's function method, LSGF, recently developed by Abrikosov *et al*[17], embeds the LIZ in a coherent potential medium [6].

The coherent potential approximation, CPA, is a mean field theory for configuration averaged quantities in random solid solutions. In the CPA, an initially random alloy is replaced with an ordered lattice of effective scatterers, thus restoring the ideal periodicity of the problem. The properties of effective scatterers are determined self-consistently from the condition that the individual atoms of the alloy, when substituted into the effective medium as impurities, do not scatter electrons on average. The method gives in general a satisfactory description of random alloy properties, including Fermi surface effects. However, as a result of the single-site approximation in CPA, most *real* space aspects (local environment, short-range order effects and so on) are lost. Nevertheless, the CPA effective medium seems to represent the alloy properties rather satisfactory on the average.

There are several possible selections for the surrounding CPA medium, for example, the single-site scattering matrices could be taken from a totally independent self-consistent CPA calculation. However, the authors of the LSGF adopted the pro-

cedure of computing the CPA medium using a number of components equal to the number of atoms in the large unit cell used for the LSMS. At each LSMS iteration, the medium is recalculated. For example, a 64 atom cell might be used to model a fcc binary random alloy; in such a case a 64 component fcc CPA calculation would be used to determine the medium. Each atom in the cell would be considered a component with concentration $\frac{1}{64}$.

With the LSGF, energies of mixing of solid solutions are converged to tenths of mRy with LIZs of only one or two atomic shells. This rapid convergence can be attributed to the fact that the CPA does an excellent job of representing the scattering in random alloys. The LSGF provides a convenient way to include the influence of short range order and charge transfer on alloy stability. However, it does not perform as well in the calculation of energies of formation of ordered compounds. This weakness indicates that its performace should be closely monitored for systems, not necessarily ordered, that differ significantly from random solid solutions. This is not surprising; the CPA is not expected to provide such a good representation of the scattering of systems other than solid solutions. Furthermore, there are situations such as amorphous materials, solid solutions with displacement short range order, and surfaces where it is not feasible to embed the LIZ in a CPA medium of a simple ordered lattice.

We propose an alternative approach, the block diagonal approach, BDA, in which the LIZ be surrounded by an additional set of atoms, which we refer to as the sur-

rounding LIZ, SLIZ. This approach is straightforwardly applicable to all structures. In the BDA, all scattering paths that traverse atoms only within the LIZ are included in determining the electron density of the central atom. All scattering paths between the LIZ and SLIZ are also included. However, some paths between atoms in the SLIZ are excluded. By excluding certain catagories of scattering paths we can reduce a large part of the KKR matrix to block diagonal form. A matrix of this form can be inverted much faster and requires much less memory. This is accomplished by dividing the SLIZ into several zones; all scattering paths that cross from one zone to another are excluded. There are many possible ways to select the LIZ, SLIZ, and zones within the SLIZ. We have chosen a simple procedure. All atoms inside a sphere of radius r_{LIZ} are in the LIZ. All atoms outside the LIZ and within a sphere of radius r_{SLIZ} are in the SLIZ. Rays are defined that emanate from the central atom and pass through the corners of a regular polyhedron. For 4, 6, or 8 zones a tetrahedron, octahedron, or cube are used, respectively. An atom belongs to the zone, associated with the ray to which it is closest. There is freedom in choosing the orientation of the polyhedron. We pick orientations that balance the number of atoms in each zone for each shell of atoms.

4.1 The block diagonal approach

In this section we will discuss the BDA in more detail and give examples of its application with comparison to other calculations. The three logical comparisons

would be to exact results, the LSGF, and the standard LSMS unsupplemented with an embedding medium. This is what we have done but with a few caveats. In the LSMS, exact results for a muffin-tin Hamiltonian are approached as the LIZ size goes to infinity. We assume that exact results are well represented by taking a very large LIZ (more than 200 atoms). Futhermore, we have avoided the work of developing a LSGF code by using the average t-matrix approximation instead of the more complicated CPA for the embedding medium. We refer to this method as the ATA-LSGF.

In the region beyond the LIZ each scatterer is replaced by the average t-matrix where the average is over all the sites in the unit cell. This differs from the LSGF method only in that the average t-matrix, t_{ATA}, is used instead of the CPA t-matrix. The two are expected to give very similar results in the examples described here. A complete discussion of the averaged t-matrix approximation had been given by Beeby [49]. Once all scatterers outside the LIZ have been given identical t-matrices, the multiple scattering problem becomes one of a periodic array of scattering centers with a localized defect cluster. The scattering path operator for the periodic system, τ_{ATA}, can be calculated using conventional "k-space" methods. This path operator can then be used to calculate the site diagonal scattering path operator for the system with the localized defect [50] according to the equation:

$$\tau = [t^{-1} - t_{ATA}^{-1} + \tau_{ATA}^{-1}]^{-1} \tag{52}$$

Our intent at the time of this work is not to implement a production version of the

ATA-LSGF but to use it as a gauge of the accuracy of the BDA. For this purpose we found it pragmatic to simply define a very large region around each atom (we will refer to it as ATA-LIZ) that consists of the true atomic scatterers of number M inside the LIZ and all other sites out to a very large distance (the ATA-LIZ) having t_{ATA} assigned to them. This is an inefficient manner to implement the ATA-LSGF but it is fine for our testing purposes as long as the ATA-LIZ is large enough to approach convergence. From previous work comparing the ATA to the CPA and from published results of Abrikosov *et al* [17, 18] that compare the ATA-LSGF and LSGF, we are confident that for the materials studied here comparison to the ATA-LSGF, implemented as described above, provides us with an adequate comparison to the LSGF.

In the BDA only a small region, the exact LIZ, ELIZ, around the central atom (a few shells of neighbours) is treated exactly, while an outer surrounding region, SLIZ, is divided into n blocks and the direct scattering effects between atoms in different blocks are completely neglected. All scattering effects between the ELIZ and SLIZ are included. This procedure leads to a great number of zero off-diagonal subblocks in the matrix $\mathbf{1} - \underline{\mathbf{T}}_{\mathbf{M}}^{-1}(\{\xi\}_{\mathbf{i}};\epsilon)\underline{\mathbf{G}}_{\mathbf{M}}(\mathbf{i};\epsilon)$. The next step is to rewrite this matrix in block-diagonal form so that we can easily take advantage of its sparse form. The block-diagonalization can be achieved by a proper relabeling atoms in the SLIZ, which leads to the row and column interchanges in the matrix. Recall that for each atom a large inverse is being performed but that only the elements of the inverse

that are diagonal in the atom index of the atom at the center of the LIZ are needed to construct its charge density. If we require only part of the inverse of a matrix, which we can take to be its upper left corner subblock elements corresponding, for example, to the cental atom or the ELIZ we can exploit the general relation:

$$\left[M^{-1}\right]_{11} = \left[\left[\begin{array}{cc} M_{11} & M_{12} \\ M_{21} & M_{22} \end{array}\right]^{-1}\right]_{11} = \left[M_{11} - M_{12}M_{22}^{-1}M_{21}\right]^{-1}. \tag{53}$$

We see that the elements of interest can also be found as a result of inversion of a much smaller matrix. In the BDA, we take M_{11} to be the ELIZ so that we can take advantage of the special block diagonal form of M_{22}. Because we neglect all scattering between the n regions on the SLIZ, each region contributes only a diagonal block A_i to M_{22} and all off-diagonal blocks are zero. Therefore, M_{22} has a completely block-diagonal form that can be inverted rapidly.

$$M_{22} = \left(\begin{array}{cccc} A_1 & 0 & & O \\ 0 & A_2 & & \\ & \ddots & & \\ & & A_{n-1} & 0 \\ O & & 0 & A_n \end{array}\right)$$

$A_1, A_2, \cdots, A_n$ are square matrices. In the BDA the term, $-M_{12}M_{22}^{-1}M_{21}$, is the embeding medium into which the ELIZ, M_{11}, is embedded. In this way the main goals of BDA are acheived. We can make use of a medium based on very many

surrounding atoms because of the efficiency of the inversion for block diagonal matrices.

If one attempted to perform by brute force a standard LSMS including as many atoms one would run into limitations of computer time and memory. There are three advantages of the BDA compared to the conventional LSMS with a very large LIZ. The time required for calculating of inverted elements in the M_{11} is given by

$$T_{BDA} = \begin{cases} \alpha_{QMR} N_{in}^2 + n(\alpha_{LU}(\frac{N_{out}}{n})^3 + \alpha_{sub} N_{in}(\frac{N_{out}}{n})^2 + \alpha_{mult} N_{in}^2 \frac{N_{out}}{n}), \\ \alpha_{LU} N_{in}^3 + n(\alpha_{LU}(\frac{N_{out}}{n})^3 + \alpha_{sub} N_{in}(\frac{N_{out}}{n})^2 + \alpha_{mult} N_{in}^2 \frac{N_{out}}{n}), \end{cases}$$

where N_{in} and N_{out} are the sizes of square matrices M_{11} and M_{22}, respectively; n is the number of blocks M_{22} is divided into, α_{QMR} and α_{LU} are numeric coefficients of QMR and LU matrix inversion methods, α_{sub} and α_{mult} are numeric coefficients for substitution and multiplication subroutines. On the other hand, the conventional LSMS spends for finding the same elements the time period

$$T = \begin{cases} \alpha_{QMR}(N_{in} + N_{out})^2, \\ \alpha_{LU}(N_{in} + N_{out})^3. \end{cases}$$

Therefore, the first achievement of the BDA is to decrease the computation time by an order of magnitude in typical situations (see Figure (2)). Secondly, there are additional time savings, because there is no need to calculate subblocks that are going to be zeroed. Thirdly, the BDA requires much less memory.

In the BDA, even after one applies the relation (53) to the inversion of matrix M, the resulting matrix $M_{11} - M_{12}M_{22}^{-1}M_{21}$ can still require significant time to invert. We can reduce this time by repeated application of relation (53) dividing M_{11} into

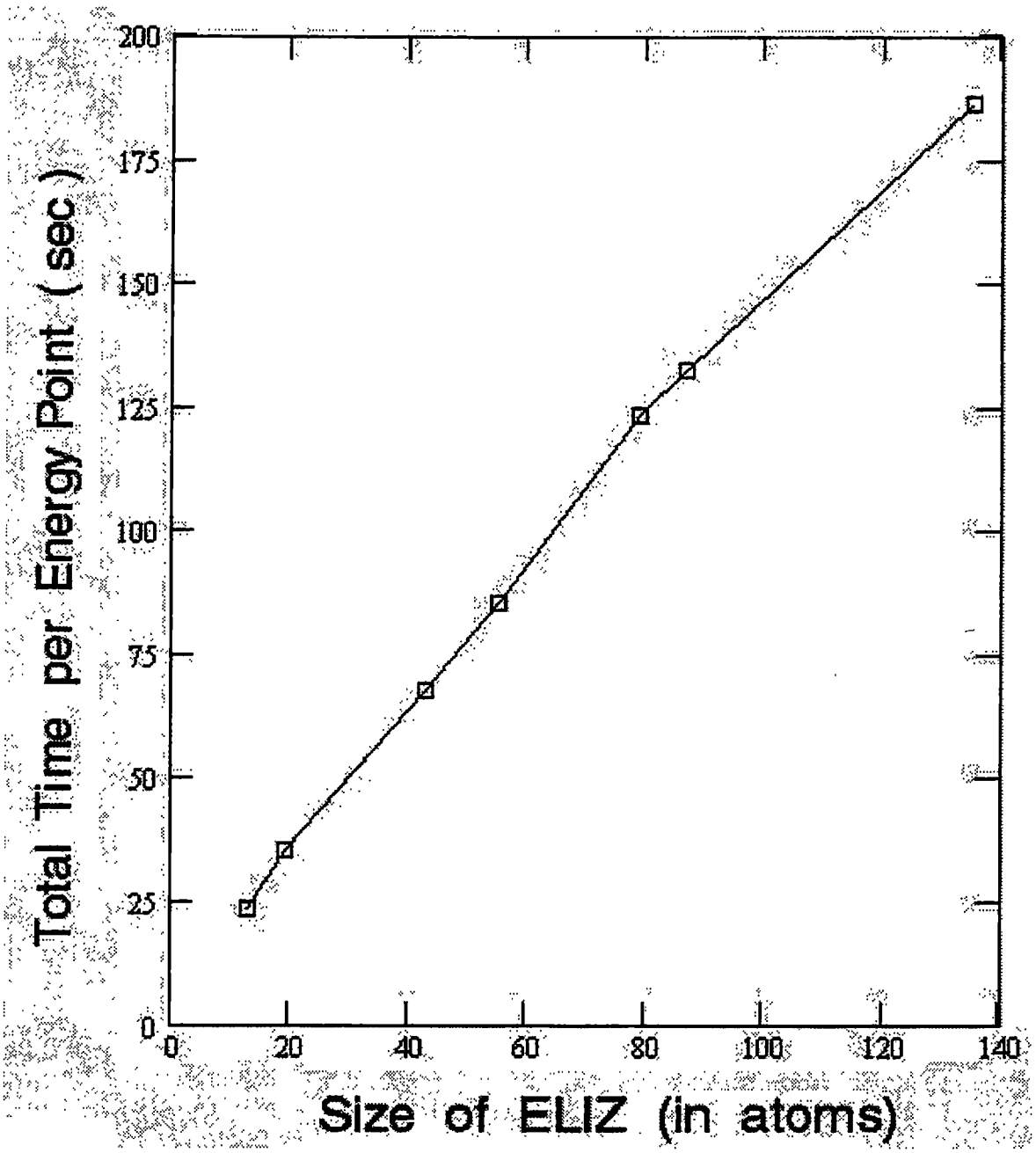

Figure 2: Time required for the inversion.

3 or 4 partitions. This simple innovation yields at least 30% speed-up in LSMS or BDA calculations. Let M_{11} be this small block and M_{22} be divided into n subblocks. Then the relation (53) is exploited n times until the new matrix of the same size as M_{11}. At this point, the only step left is to invert that newly calculated matrix. As can be seen from Figures (3) and (4), the above-described process is optimized if $n = 3$ or $n = 4$.

The path operators in MST can be analytically continued to complex energy. It can be shown that they are analytic in the upper half of the complex energy plane. This property is maintained in the LSMS, because the path operator includes all scattering from a perfectly reasonable cluster of atomic scatterers. However, the path operator in the BDA although based on a similar but typically larger cluster does not include some scattering paths. It is well known, from attempts to construct effective scattering theories for disordered systems, that selectively excluding scattering paths can result in non-analytic behavior and negative densities of states. One of the important features of the CPA is that it is guaranteed to have the appropriate analytic behavior and positive density of states. For the BDA, there are no such guarantees. Some comfort can be taken in the fact that as the ELIZ is made larger proper analytic behavior must be approached as the size of the SLIZ goes to zero. For large ELIZ we can assume that the poles of the path opperator are not far from their limiting positions. Even in this case, it would be unwise to rely on results for energies near the real axis where a pole may be spuriously displaced into the positive

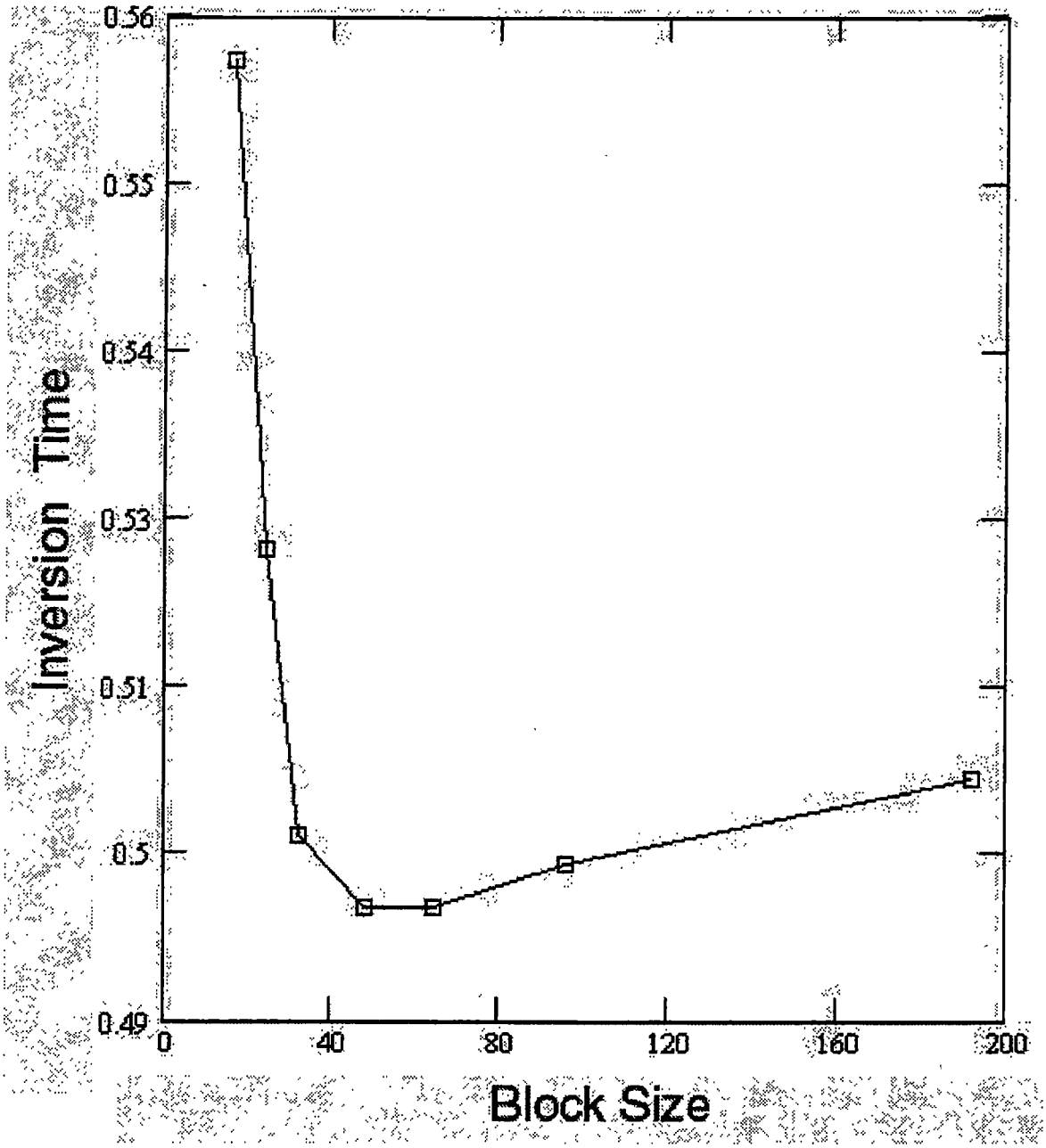

Figure 3: Time in seconds required for the inversion of matrix with 192 rows.

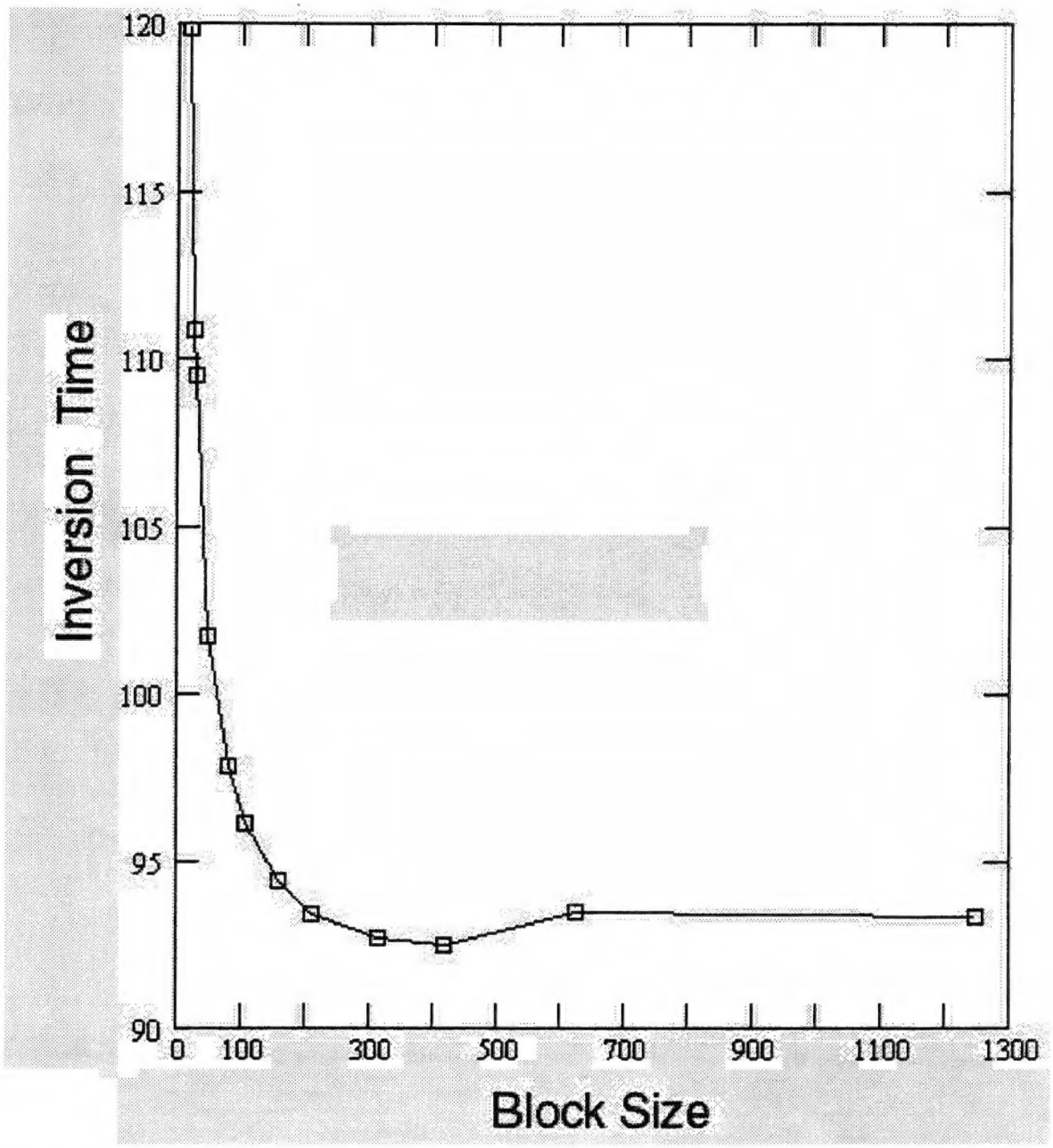

Figure 4: Time in seconds required for the inversion of matrix with 1248 rows.

half plane by the BDA. Fortunately, in almost all cases calculations can be avoided near the real axis where troublesome behavior may occur.

In practice, the quantity calculated in the LSMS is the diagonal part of the Green function at a set of complex energies, $\{z_i\}$. For calculations at zero temperature the z_i are points of a contour integration mesh that begins on the real axis below the bottom of the valence band and ends on the real axis at the Fermi energy. At finite temperature, T, the z_i may include both points on a contour of integration and poles of the occupation function. There are many possible choices for z_i; for us, the important distinction between finite and zero temperature is that, at finite temperature, none of the z_i needs to be near the real axis. The imaginary part of z_i can always be greater than $\pi K_B T$.

Let us demonstrate the behavior of the poles in the BDA for the one-dimensional model of δ-function potentials, namely,

$$V(x) = -\sum_n \lambda\delta(x - na). \tag{54}$$

In this simple model results can be obtained analytically. For example, if the ELIZ is chosen to be only the central site and the LIZ has in addition only the two neighboring sites, the site diagonal scattering path operator on the central site has poles at:

$$E_1 = -\frac{1}{4}(3 + 2\sqrt{2})\lambda^2 \tag{55}$$

and

$$E_2 = -\frac{1}{4}(3 - 2\sqrt{2})\lambda^2. \tag{56}$$

These poles are not located in the upper half plane so that the proper analytic behavior is maintained for this example. The BDA poles can be compared to the conventional LSMS using a three site LIZ. The LSMS poles are:

$$E_1 = -\lambda^2 \tag{57}$$

and

$$E_2 = -\frac{\lambda^2}{4}. \tag{58}$$

They don't lie in the upper part of complex plane as was guaranteed.

We have performed many self-consistent calculations with the BDA and have not observed any anomalous behavior that we might associate with non-analitic behavior. In an especially difficult case, namely, pure Ni, these calculations have been performed at finite temperature in order to avoid energies near the real axis. Our view based on experiences with calculations at both zero and finite temperature is that typical energy integration contours will not be adversely affected provided adequately large ELIZs are used.

4.2 Results

Recall that our plan is to compare the BDA with exact results, the LSGF, and the LSMS with the caveats discussed above. Our first example is Cu-Zn which has been a proving ground for theories of substitutional disorder. It is known that the CPA works very well for this system. We have modeled the Cu-Zn alloy with the

lattice constant a = 6.90 a.u. by a supercell of 4 atoms on a fcc underlying lattice at a concentration of $\frac{1}{2}$. The sites were occupied according to the $L1_0$ structure which is the quasi-random structure for the 4 atom case on this lattice at this stoiciometry. It has the same first nearest neighbor coordination as the random alloy.

Firstly, we obtained what we consider essentially exact results by using a large local interaction zone of 201 atoms (ten shells). Secondly, the BDA was applied for a series of successively larger ELIZs. In all of these BDA calculations the total LIZ was taken to contain 201 atoms. Observe that as the LIZ increases convergence to the "exact" result is guaranteed and, therefore, the ultimate convergence should not be used as a measure of the merit of the BDA. Thirdly, the ATA-LSGF was computed using a series of successively larger LIZs; the atoms beyond the LIZ but within the 201 nearest atoms were replaced by ATA single-site t-matrices. Again, ultimate convergence is guaranteed. Finally, the standard LSMS was applied for a series of successively larger LIZs. Once again, convergence is guaranteed. In all cases the calculations were self-consistent muffin-tin calculations. The convergence with respect to the size of the ELIZ or LIZ has been studied within three techniques, namely, the BDA, ATA-LSGF, and conventional LSMS. In Fig. 5 we present the total energies of the ordered fcc Cu-Zn alloy as a function of ELIZ for the BDA and LIZ size for the ATA-LSGF and LSMS. One can easily see that while the LSMS converges very slowly with respect to the size of LIZ, the ATA-LSGF and BDA converge much faster with about the same accuracy of less than 0.1 mRy beginning

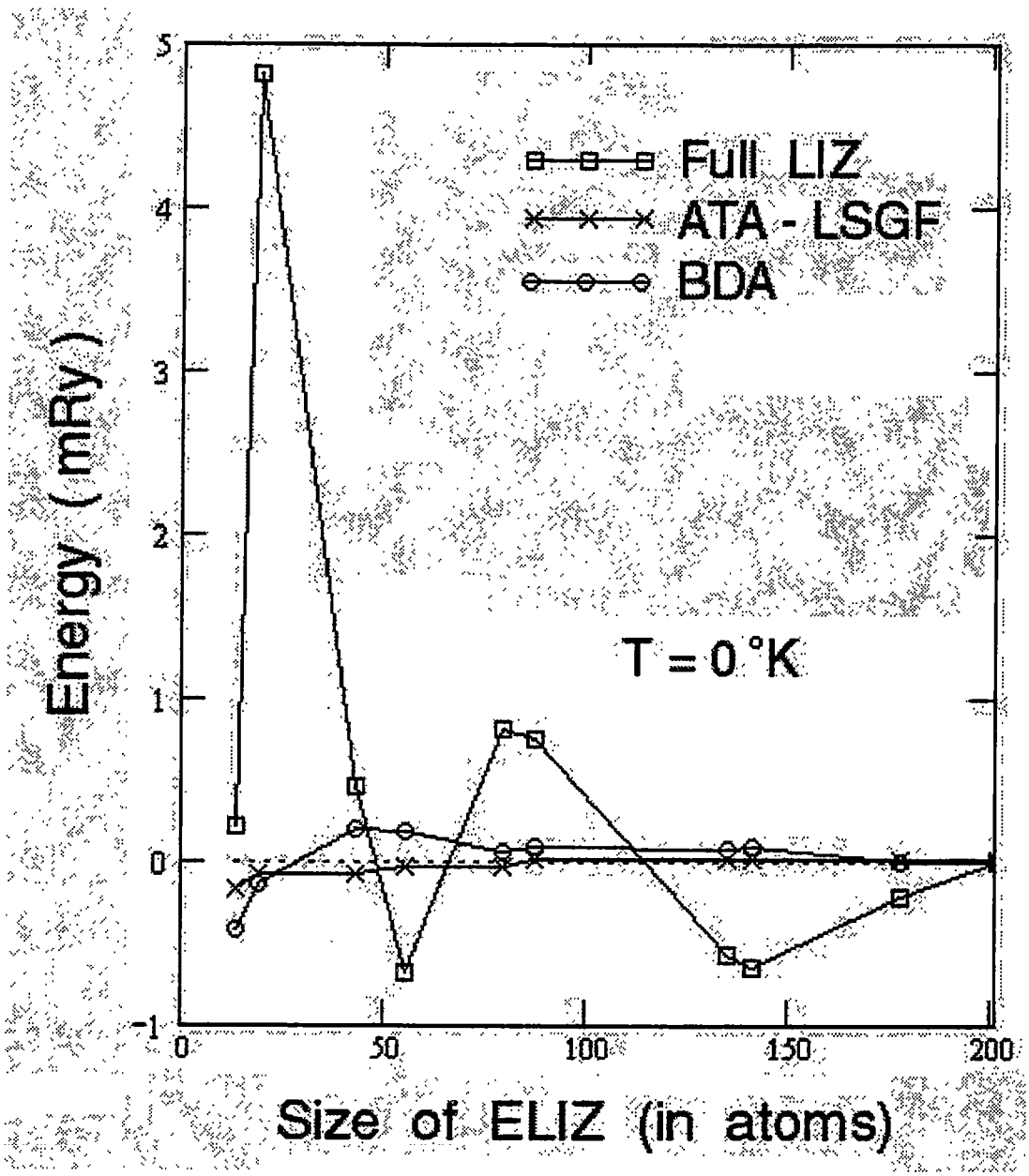

Figure 5: Total energy of fcc CuZn(a = 6.90 a.u.) as a function of ELIZ size.

with the second shell (19 atoms). For the same level of energy convergence, the BDA consumes much less CPU time than the LSMS and has a CPU consumption similar to that of an efficiently implemented ATA-LSGF or standard CPA based LSGF.

Next we discuss the case of ordered bcc NiAl alloy with a= 5.45 a.u., which has been modeled by a supercell of two atoms. We performed the same sets of calculations as for Cu-Zn but we took the "exact" result to be achieved with an LIZ equal to 229 atoms(twelve shells) for all energy points. Again, a somewhat slow convergence of conventional LSMS with LIZ size can be seen in Fig. 6 . At the same time, the BDA converges much better than the ATA-LSGF. In fact, it does not become clear that the ATA-LSGF converges at all until we have obtained results for more than 8 shells. We note that NiAl is hard to converge at zero temperature because of somewhat steep profile of its density of states near the Fermi level.

A more difficult test case is provided by bcc Mo for which the chemical potential falls in the middle of the *d*-band complex. The lattice constant for this metal a= 5.80 a.u. We made the total size of the LIZ, which defines our "exact" result, be equal to 259 atoms (13 shells) for all energy points. One can see in Fig. 7 that the conventional LSMS converges very unacceptable at zero temperature. It shows a new peak in the total energy when the LIZ includes 8 shells. This peak was not detected earlier in [14] because they mistakenly assumed near convergence at a smaller LIZ. To the contrary, the BDA does an excellent job for this material. It converges pretty fast without having sharp peaks. Because there is only one

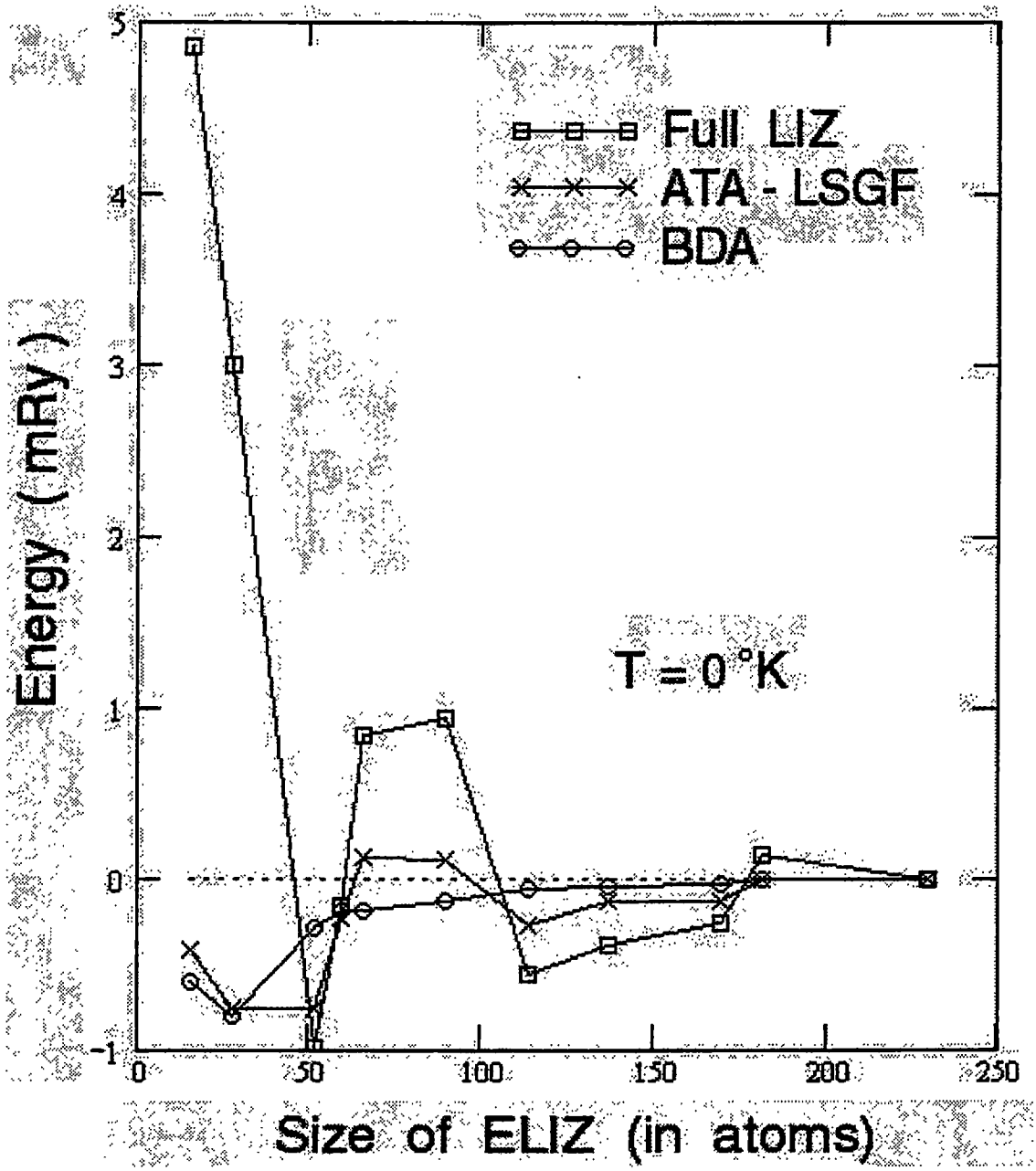

Figure 6: Total energy of bcc NiAl(a = 5.45 a.u.) as a function of ELIZ size.

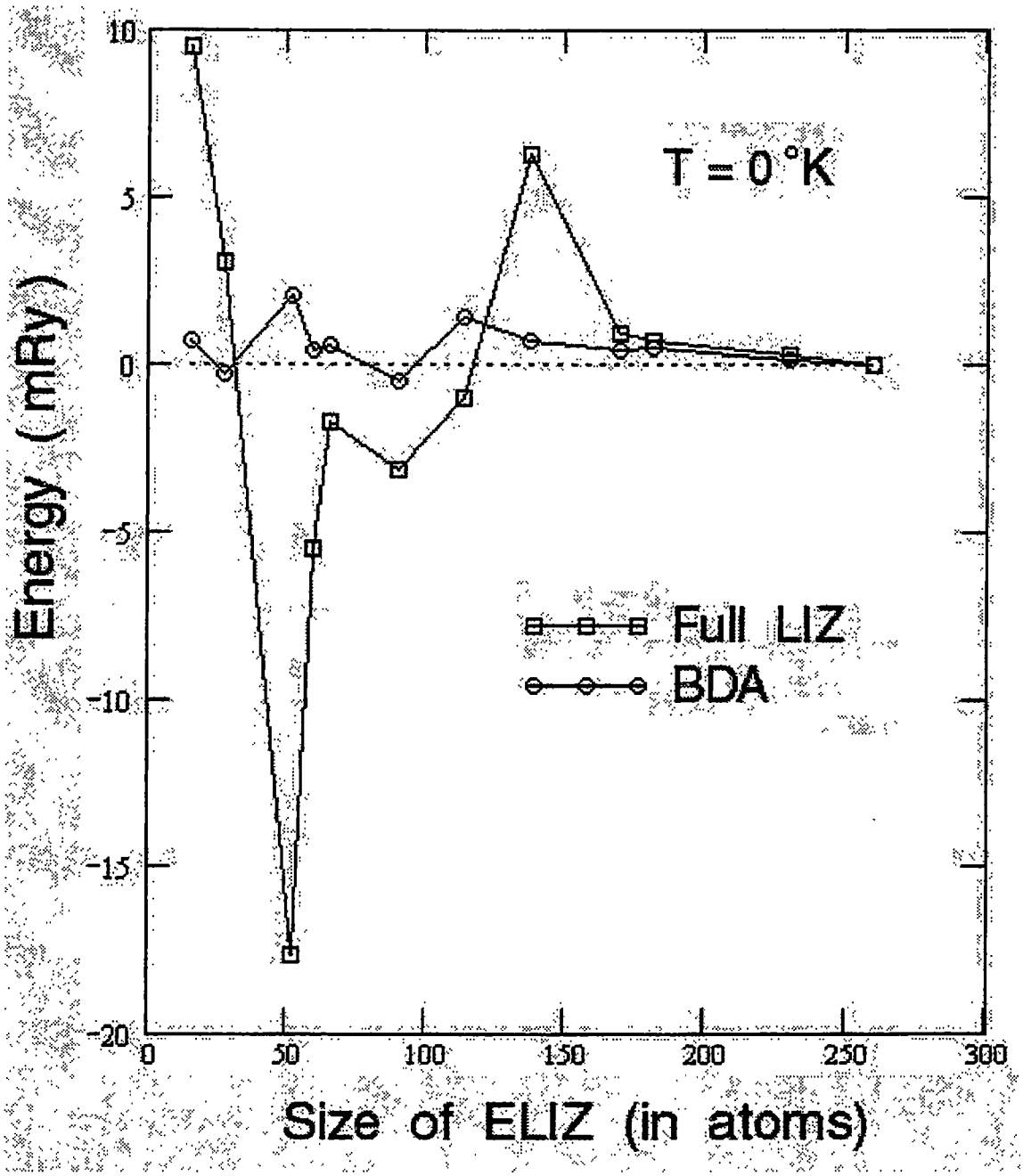

Figure 7: Total energy of bcc Mo(a = 5.80 a.u.) as a function of ELIZ size.

component, the ATA-LSGF is exactly equal to the LSMS result for an LIZ of 259 atoms.

To test the BDA for pure fcc Ni, which has a density of states that decreases most abruptly near Fermi level at zero temperature, we take advantage of the finite temperature, T, Harris-Foulkes-like [51, 52] free energy functional, F_H, developed by Nicholson *et al* [48]. This functional is stationary with respect to the occupation function $f(\epsilon - \mu)$ and T, as well as to all of parameters that specify it. The former property allows us to use the approximate *conduction band* Fermi function of Nicholson *et al* [48] to enable the efficient calculation of $F_H(T)$ at large fictitious electron temperatures, whilst the latter allows the $F_H(T)$ calculated at these temperatures to be extrapolated back to $T = 0°K$, thereby permitting the ground state energy to be evaluated. Thus we can compare the results of three different methods, namely, the conventional LSMS and the DLM (disordered local moments)-LSGF-ATA and the BDA, for the total free energy of Ni with the lattice constant a= 6.65 a.u. in Fig. 8. The size of the LIZ that defines the "exact" result was chosen to be equal to 135 atoms (7 shells) for all energy points. It is clear that the BDA converges to an accuracy of better than 0.1 mRy with only two shells included, while the DLM-LSGF-ATA demonstrates signs of lack of convergence even after six or seven shells are included. This can be explained if one compares the embedding medium in these two techniques with respect to the presence of magnetic moments at their sites. While all sites in the BDA SLIZ have nonzero moments aligned ferromag-

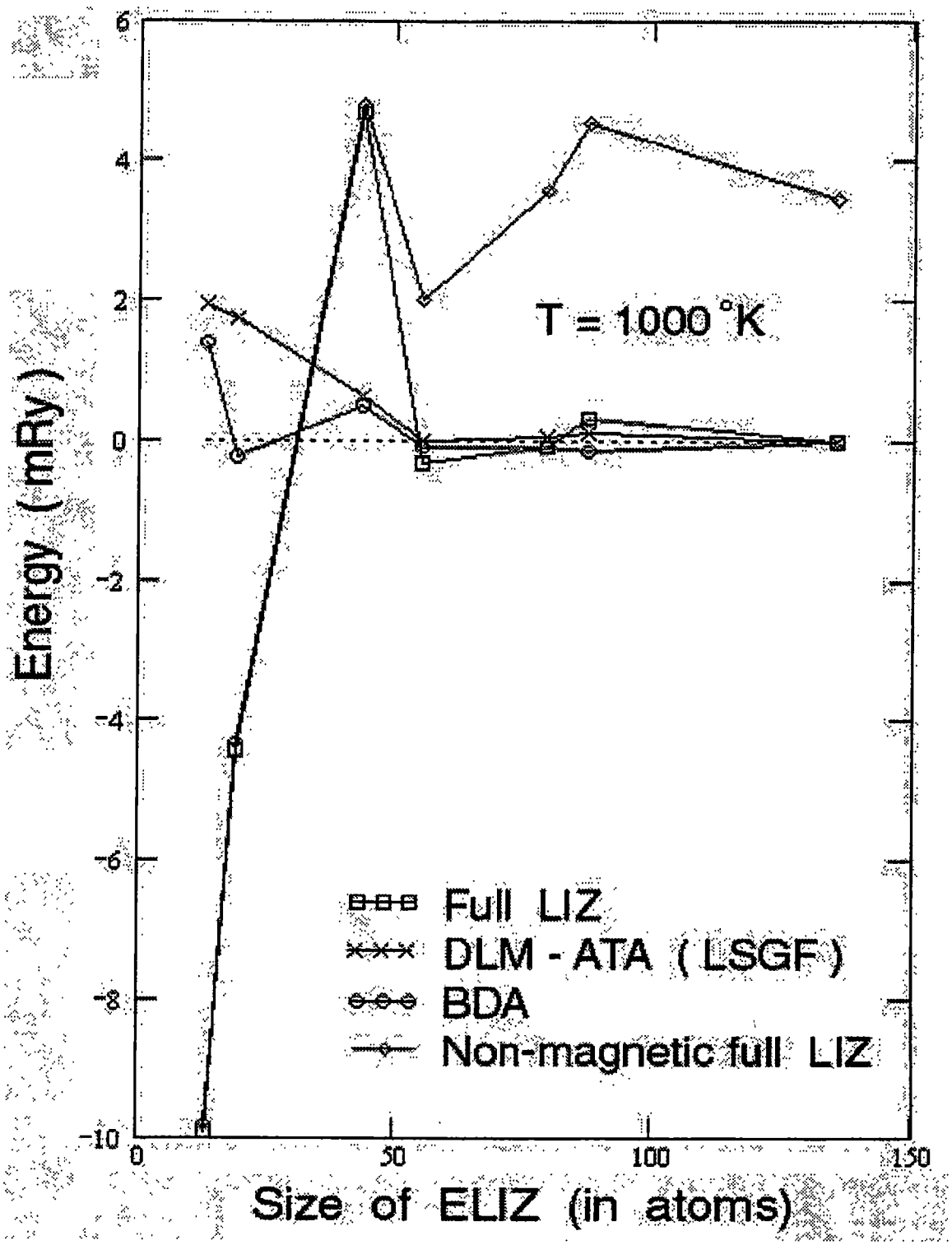

Figure 8: Total energy of fcc Ni(a = 6.65 a.u.) as a function of ELIZ size at $T = 1000° K$.

netically with the moments in the ELIZ, the ones with the DLM-LSGF-ATA have no moment on average. The iteration processes for the DLM-LSGF-ATA and BDA methods cannot also be converged at zero temperature. The conventional LSMS iterations converge at zero temperature. However, the LSMS converges with respect to the size of the LIZ only with seven or more shells included as can be seen in Fig. 8.

From the point of view of the conventional LSMS, the magnetic moment at an atomic site has nonzero value with at least four shells included, as shown in Fig. 9. To the contrary, in the DLM-LSGF-ATA and BDA methods the very first shell is enough for that. As one can see, the latter converges better than the former. Of course, the conventional LSMS iterations converge even at zero temperature. However, its convergence with respect to the size of the LIZ is even worse than at T = 1000° K. The Fermi energy calculated in four different approaches is shown in Fig. 10. The total size of the ELIZ and SLIZ was the same in last two Figures as in Fig. 8.

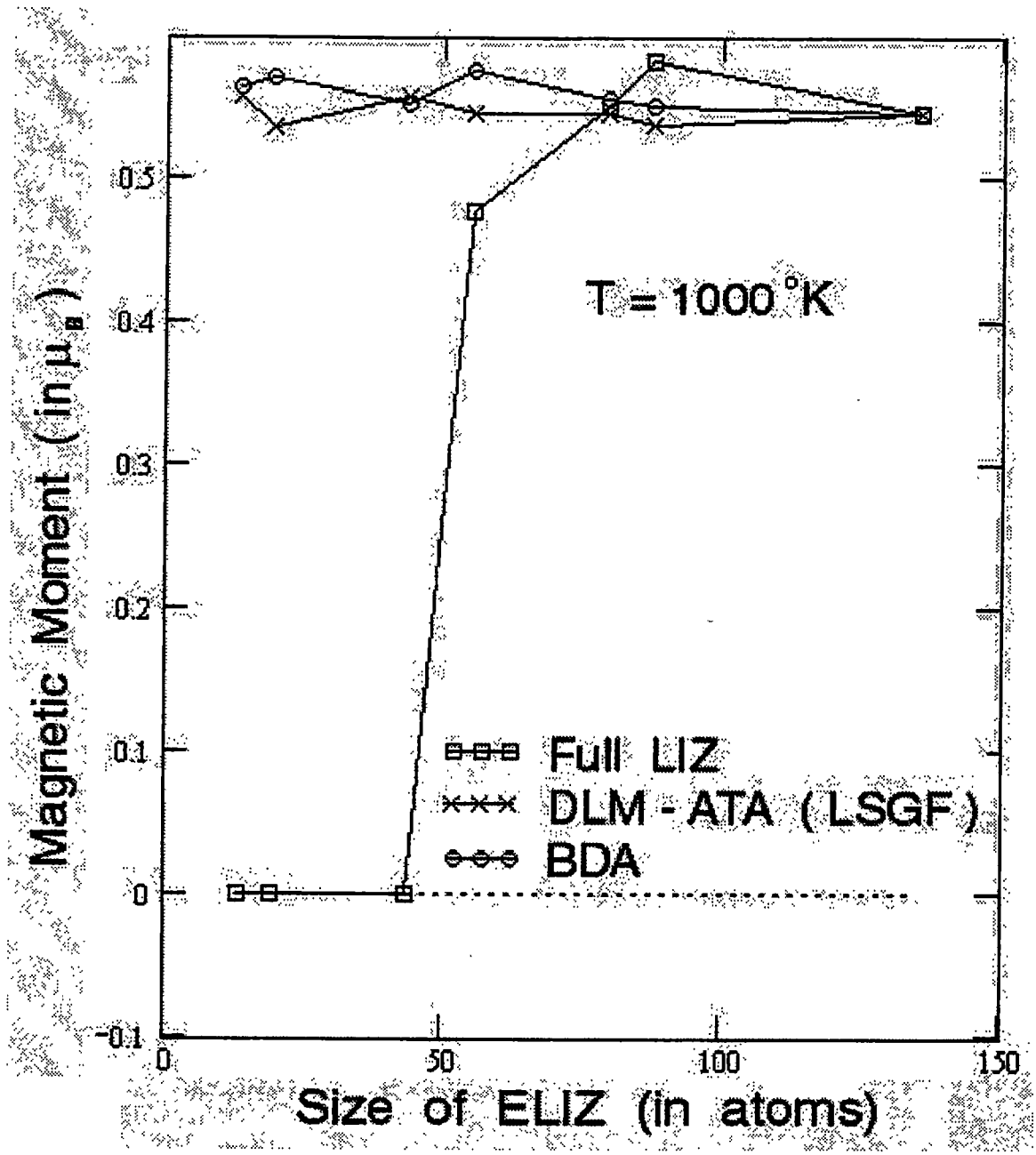

Figure 9: The magnetic moment per atom of fcc Ni (a = 6.65 a.u.) as a function of ELIZ size at $T = 1000°K$.

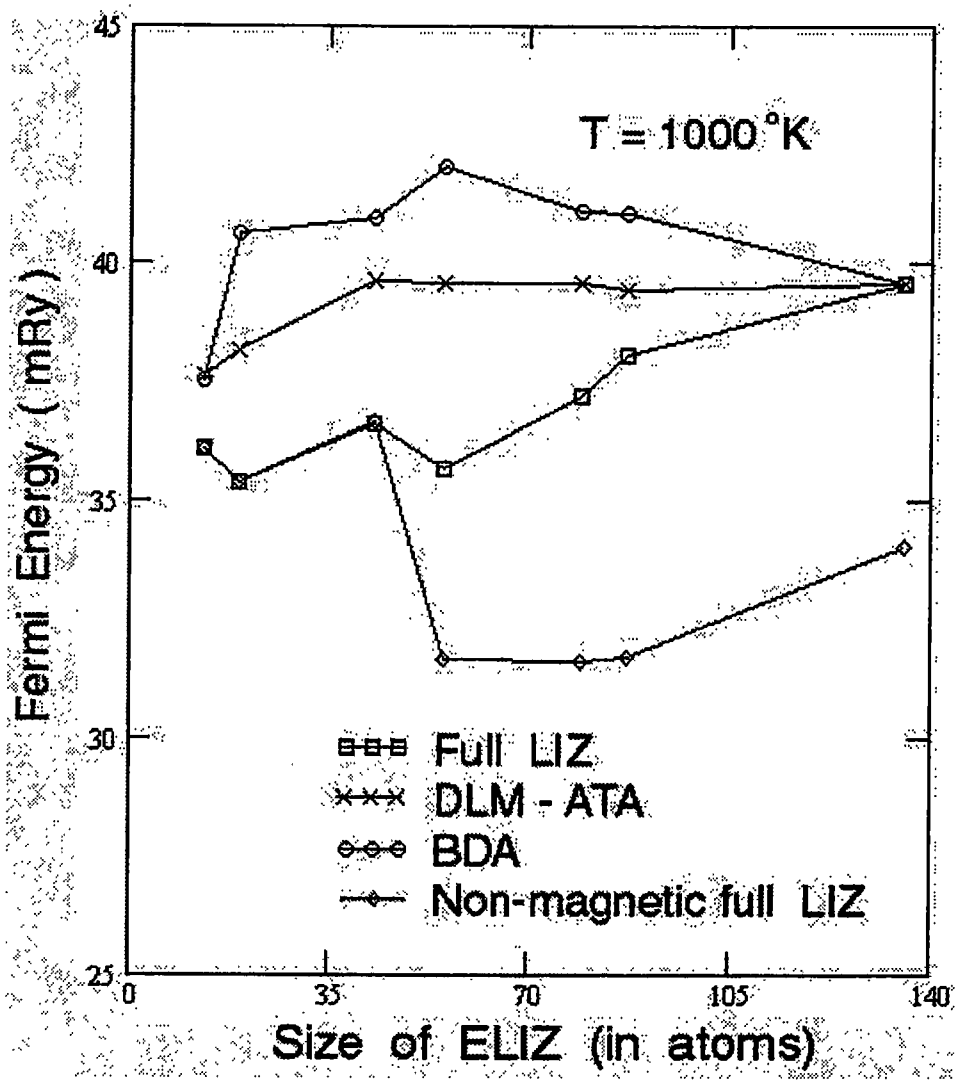

Figure 10: The Fermi energy of fcc Ni (a= 6.65 a.u.) as a function of ELIZ size at $T = 1000°K$.

Chapter 5

Application to CuPy Interface

Recently there has been great interest in the transport properties of magnetic materials which are inhomogeneous on the scale of the electronic mean free path. This interest has arisen because of the discovery of a new form of magnetoresistance called giant magnetoresistance (GMR). GMR is a change (usually a pronounced decrease) in the electrical resistance of an inhomogeneous system that is observed when an applied magnetic field causes an alignment of the magnetic moments in different parts of the material. GMR has been observed in several geometries. It was first observed in artificially layered systems [53, 54]. Later, it was observed in systems consisting of magnetic inclusions in a non-magnetic matrix [55, 56]. It has also been recognized that numerous antiferromagnetic compounds exist in a natural layered structure and show a large decrease in resistivity (GMR) in the presence of a magnetic field strong enough to align their moments [57, 58].

GMR is generally considered to arise from spin-dependent scattering, that is, electrons of one spin are believed to be scattered more strongly than those of the other. Consider, for example, a hypothetical layered system consisting of layers of ferromagnetic metal, F, alternating with layers of normal metal N, and with current flowing perpendicular to the layers. Suppose, further that the majority spin electrons are hardly scattered in the ferromagnetic material whereas the minority spin

electrons are very strongly scattered. Suppose further that the potentials seen by the majority electrons hardly differ between the F and N layers while the atomic potentials seen by the minority spin electrons in the F and N layers are quite different. We would expect that such a system would show a much larger conductivity when the F layers are aligned parallel than when neighboring F layers are aligned antiparallel because in the case of parallel alignment the majority spin electrons experience an effective short-curcuit [59].

A giant magneto-resistance (GMR) spin valve consists of two ferromagnetic layers separated by a thin layer of nonmagnetic metal. These three layers are mounted on an antiferromagnetic substrate that pins the moment direction in the adjacent ferromagnetic layer. There can be a large change in the electrical resistivity when an external magnetic field flips the orientation of the magnetization of the free layer relative to the pinned layer.

Spin valves have possible application in magnetic read heads, magnetic sensors, and non-volatile magnetic memory. The magnetically soft $Ni_{0.8}Fe_{0.2}$ solid solution known as permalloy, Py, is a leading candidate for the ferromagnetic material. Cu or Cu alloys are common choices for the non-magnetic layer. The GMR ratio depends not only on the choice of materials for the layers but also on their thickness and on the details of the interfaces between them. For example, it has been observed that the placement of less than a monolayer of Co at the ferromagnet-metal layer interface significantly improves the GMR ratio in Py/Cu/Py spin valves [28].

The importance of the interface is also evident in the reduction of GMR ratios caused by annealing [28]. This reduction is usually ascribed to anneal induced interdiffusion at the interfaces. Also associated with interdiffusion are so called magnetically dead layers that occur when a thin magnetic layer is sandwiched between nonmagnetic layers. It is observed that there is a minimum number of atomic planes of magnetic material below which the magnetic planes have no magnetization[28]. Above this minimum number of atomic planes the moment increases linearly with the number of planes and the increase per plane is equal to the magnetization associated with a plane in the bulk magnetic material. It is known that magnetically dead layers are very detrimental to GMR. It is therefore important to understand this phenomenon and search for ways to avoid its occurrence.

5.1 Model Construction

Ni differs from Fe and Co in that it loses its moment as a substitutional impurity in Cu. At low temperature, the solid solution moment per atom is observed both experimentally [60, 61, 62] and theoretically [63] to decrease from its value of $0.6\mu_B$ in pure Ni at about $0.1\mu_B$ per atomic fraction Cu. This decrease is due both to the dilution of Ni by Cu and to the decrease of the Ni moment, which vanishes at around 60% Cu. At room temperature the moment decreases faster, disappearing at about 30% Cu.

Let us study a model [64] in which Cu atoms migrate into the magnetic layer,

where they reduce the surrounding moments. To model interfaces with different amounts of intermixing, and to make connection to the annealing data, we consider initially abrupt interfaces that we allow to interdiffuse for increasing amounts of time, resulting in more intermixing. For Ni/Cu, the atoms are of similar size, and the equilibrium phase above 322 °C is a slightly clustering solid solution. Therefore, it is reasonable to assume that hopping probabilities are almost species independent. Thus, the concentration on a layer should obey a one-dimensional diffusion equation of the form

$$\frac{dc_k}{dt} = \sigma_D[-c_k + \frac{1}{2}(c_{k-1} + c_{k+1})], \tag{59}$$

where c_k is the concentration of Cu on the kth atomic plane and σ_D is the number of out of plane jumps per second per site. This equation is easily solved in terms of the dimensionless time, $\sigma_D t$, for an initially perfect periodic multilayer consisting of n_{Cu} planes of Cu followed by n_{Ni} planes of Ni. Unfortunately, σ_D is not available, and since the experimental deposition and annealing includes several successive temperatures, the mapping from τ to t is not even linear. However, the mapping should be independent of n_{Cu} and n_{Ni}. This allows us to qualitatively compare our calculated loss in moment and interfacial width with those obtained from magnetometry and x-ray reflectance [65].

The underlying concentration profiles are evolved from n_{Ni} perfect [111] atomic planes of Ni embedded in Cu. As τ increases, mixing occurs and the concentration profile evolves. To obtain a rough picture of the dependence of the moment on the

thickness of the Ni layer we approximate the moment on a Ni atom by the average Ni moment in a random alloy, with the same average number of Ni nearest neighbors as the Ni atom under consideration. With this assumption, the total moment can be determined as a function of intermixing, calculated from Eq. (59) for different numbers of Ni planes. In Fig. 11, we represent the total moment per unit cell of a multilayer consisting of 25 Cu planes followed by n_{Ni} planes calculated as a function of τ using the room temperature data for the moment as a function of concentration.

Armed with the moment as a function of τ we can fix the value of τ by requiring that the number of magnetically dead layers agrees with the experiment. Gurney *et al.* [29] found that at room temperature Cu/Ni/Cu has 5 magnetically dead layers; this fixed the only parameter in the simple diffusion model which then becomes applicable for any number of Ni atomic layers.

These results show that, depending on τ(i.e., intermixing), when only a few Ni layers are present, there is no moment, but as Ni layers are added, a point is reached when the moment appears; the moment then increases almost linearly. In Fig. 12, the diffusion model's net moment versus the number of Ni layers is plotted for $\tau = 5$, along with room temperature measurements. The value, $\tau = 5$, was chosen to give the best agreement with the measurements.

A system of greater practical importance is Cu/Py/Cu because it contains interfaces of the type actually used in GMR devices. Above we have described a model for Ni/Cu interfaces that relies on one parameter τ that describes the effective number

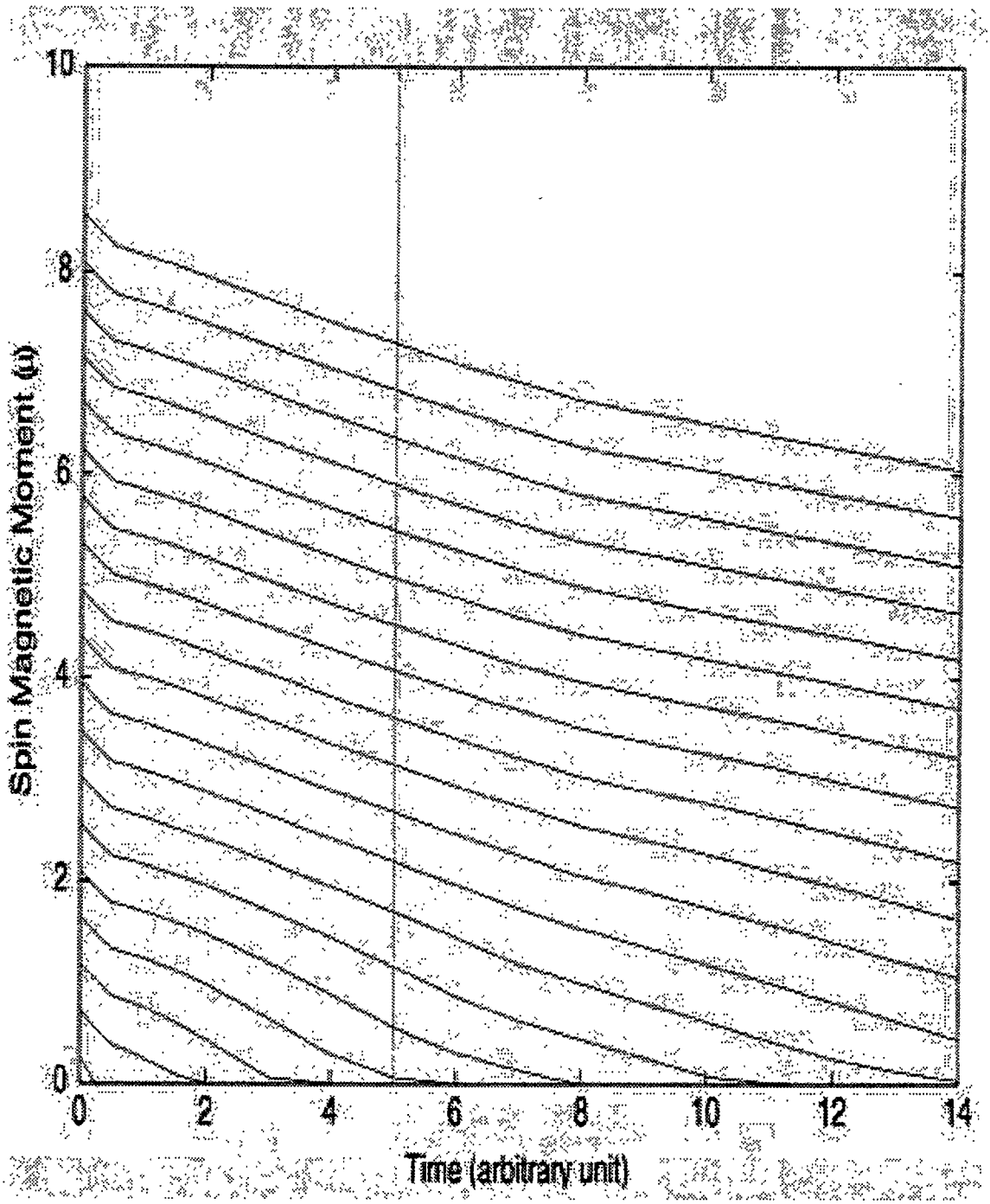

Figure 11: The total spin magnetic moment as calculated in the model is shown as a function of τ for various n_{Ni}. The number of Ni planes goes from 2 in the lower left corner to 20 at the top.

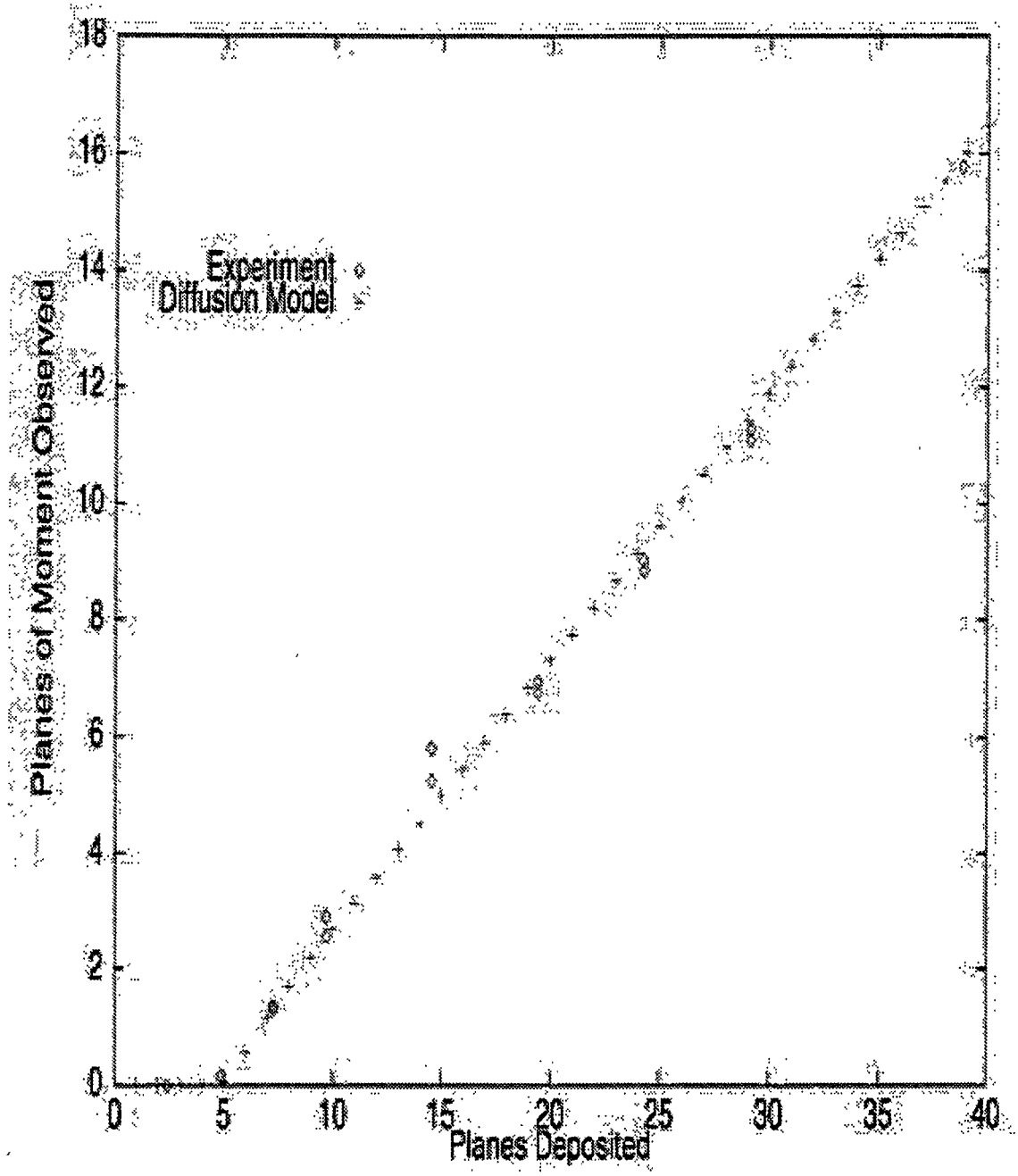

Figure 12: Magnetization (expressed in terms of an equivalent number of planes with bulk moments) versus number of planes deposited. Calculated and experimental results are shown for Cu/Ni/Cu sandwiches.

of atomic hops that take place while the interface is formed. For Cu/Py interfaces formed under similar conditions we can hope that the same value of the parameter τ will describe the interdiffusion. This can be expected to work because of the similarity in size and interactions between Fe, Ni and Cu. We, therefore, assumed that Cu, Ni and Fe have similar diffusion constants and simply replaced Ni randomly by Fe in the Cu/Ni/Cu model until concentrations appropriate to Cu/Py/Cu were obtained. To recap, we started with 5 perfect Ni layers in Cu and let the Cu and Ni diffuse until the calculated moment went to zero. This specified how long to let model configurations diffuse for an arbitrary number of Ni layers. Following the assumption that Fe diffuses at the same rate as Ni we also constructed configurations corresponding to the deposition of arbitrary amounts of Py. This model can only be valid if Py and Ni samples were sputtered under the same conditions of ion energy, substrate temperature, etc.

Zhou and Wadley [66] have also obtained atomic structures, but by atomic simulation of alternately sputtering Ni layers in Cu. They used realistic values of the energy of the impinging atoms but were forced by computational requirements to deposit material at rates that greatly exceeded experimental rates. Their simulated concentration profile closely resembles that from the simple diffusion model. Magnetic moments for the simulated model calculated with the LSMS[14] method and values calculated with the layer KKR [67] for the diffusion model agree with each other and with experiment [68]. The consistency of these results convinced us that

the diffusion model gave a reasonable model for Ni-Cu interfaces.

5.2 Results

As described above we extrapolated from Cu/Ni/Cu structures to Cu/Py/Cu structures by randomly replacing 20 % of the Ni atoms by Fe atoms. If this is a valid procedure, the calculated magnetization should agree with measured values. The saturation magnetization of Cu/Py/Cu spin-valves was calculated with the LSMS,(local interaction zone of 57 atoms), as a function of Py thickness and compared to experiment. Obviously, the magnetization at zero Py thickness is zero and at infinite thickness the derivative of the moment with Py thickness is just the magnetization of a layer of bulk Py. In addition to these two trivial data points we constructed two samples, one with nominally 2 layers and one with nominally 4 layers of Py. The first sample consisted of 8 [111] hcp layers each with 25 atoms; the second sample had 10 [111] hcp layers each with 25 atoms [34]. Periodic boundary conditions were used.

In the course of trying alternative methods for iteratively solving the Kohn-Sham equations for the 4 Py layer case we obtained four different metastable magnetic structures for the same atomic configuration. In Fig. 13 the energies of these metastable magnetic structures are plotted versus the collinearity. Energy is measured relative to the energy of the collinear case. We define the collinearity:

$$c = \frac{x - x_{\text{random}}}{1 - x_{\text{random}}} \tag{60}$$

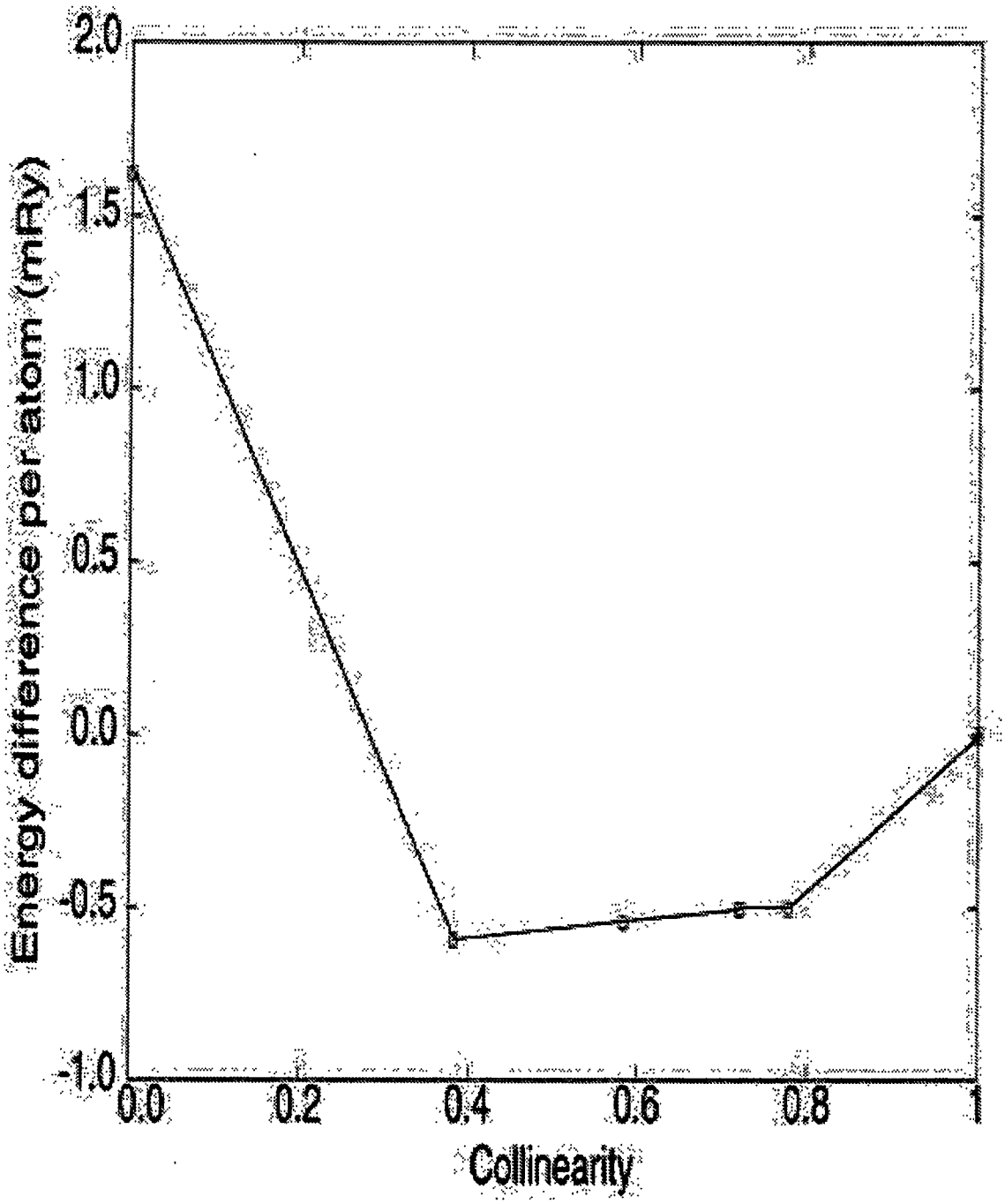

Figure 13: The energy per atom for a 250 atom model of 4 atomic planes of Py inter-diffused in Cu is shown for several levels of collinearity. The energy zero is the collinear state.

where

$$x = \left| \frac{\sum_{i=1}^{N} \mathbf{m_i}}{\sum_{i=1}^{N} m_i} \right|, \tag{61}$$

$\mathbf{m_i}$ is the vector magnetic moment on site i, and N is the number of atoms in the unit cell. The value of x_{random} is found by averaging x over many sets of moment directions chosen randomly but with the moment magnitudes kept fixed at the values appropriate for the magnetic configuration under investigation. For example, one can find that for a system with the identical moments $x_{\text{random}} = 1$, if N = 1, and $x_{\text{random}} = \frac{2}{3}$, if N = 2. The systems under investigation are described with $x_{\text{random}} \approx 0.23$. As the number of atoms in the unit cell increases the value of x_{random} goes to zero. This definition (Eq.(60)) adjusts for the fact that a small number of moments randomly oriented will have a nonzero value of x even though the infinite system being modeled would have a zero value of x if the moments were randomly oriented. We measure the collinearity using the random case as a reference. Also shown is the energy of the sample when the iteration proceeded from the initial state with randomized moment directions and the moments were not allowed to change direction. This magnetic state has roughly zero collinearity. The fact that the random configuration has an appreciably higher energy than the metastable or collinear configurations demonstrates that the correlation among the moment directions was important in stabilizing the noncollinear structure. The most significant result was that the collinear state was not stable; there was some noncollinearity due to interdiffusion at the interface.

The plot in Fig. 14 of the magnetization as function of deposited Py layers is consistent with experiment [28]. It is difficult to make definitive statements about the agreement because we have performed the calculations for only one atomic configuration at each of the Py layer thicknesses and we cannot do a full search for all metastable magnetic configurations. We infer from these calculations that other atomic configurations and other metastable magnetic structures would fall roughly in the range of those that we have thus far calculated. The magnetic structure corresponding to the lowest degree of collinearity for the 4 Py layer case is shown in Fig. 15. There appear to be pairs of moments that are ferromagnetically aligned while others have a canted relationship. These correlations are partially preserved from one metastable state to another.

Non-collinear moments are detrimental to GMR; we are thus motivated to look for additions that will promote collinearity [35]. It has been observed experimentally that a "dusting" of Co at the interface improves GMR. The reason for this improvement is not understood but makes Co a good candidate for an addition that promotes collinearity. The cobalt layer at the interface between the copper layer and the permalloy layer was thought to be advantageous in at least three ways, by increasing the contrast (compared to nickel) between the magnetic and the spacer layers in the minority channel as can be seen in Figure 16, by acting as a diffusion barrier since cobalt and copper are immiscible, and finally, by assisting in maintaining exchange coupling in the magnetic layer as illustrated in Figs. 16 and 17.

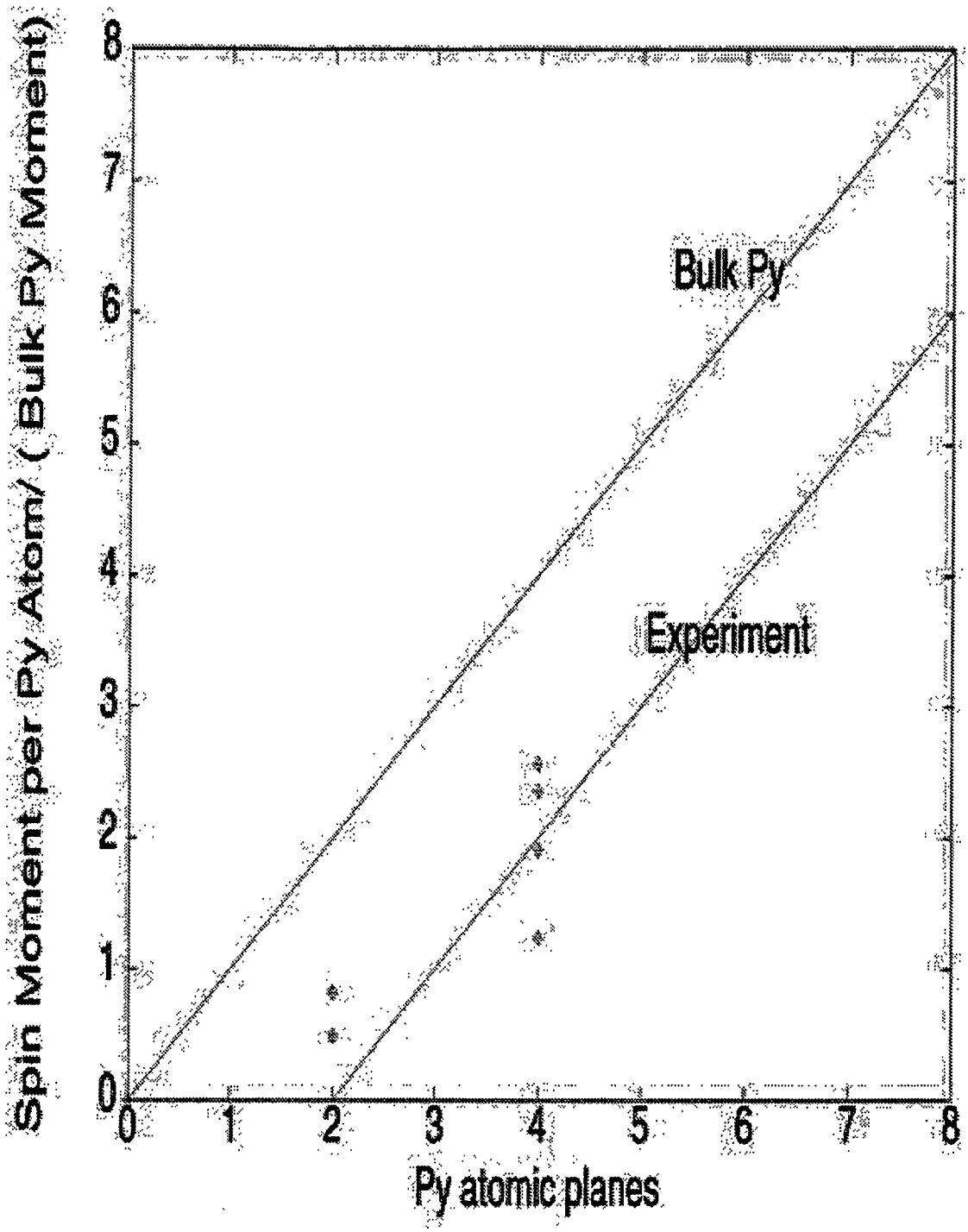

Figure 14: Total spin magnetization per Py atom in the model as a function of the number of atomic planes of Py embedded in Cu. Values are shown for several metastable magnetic configurations. The moments are given in terms of the moment per Py atom in bulk Py.

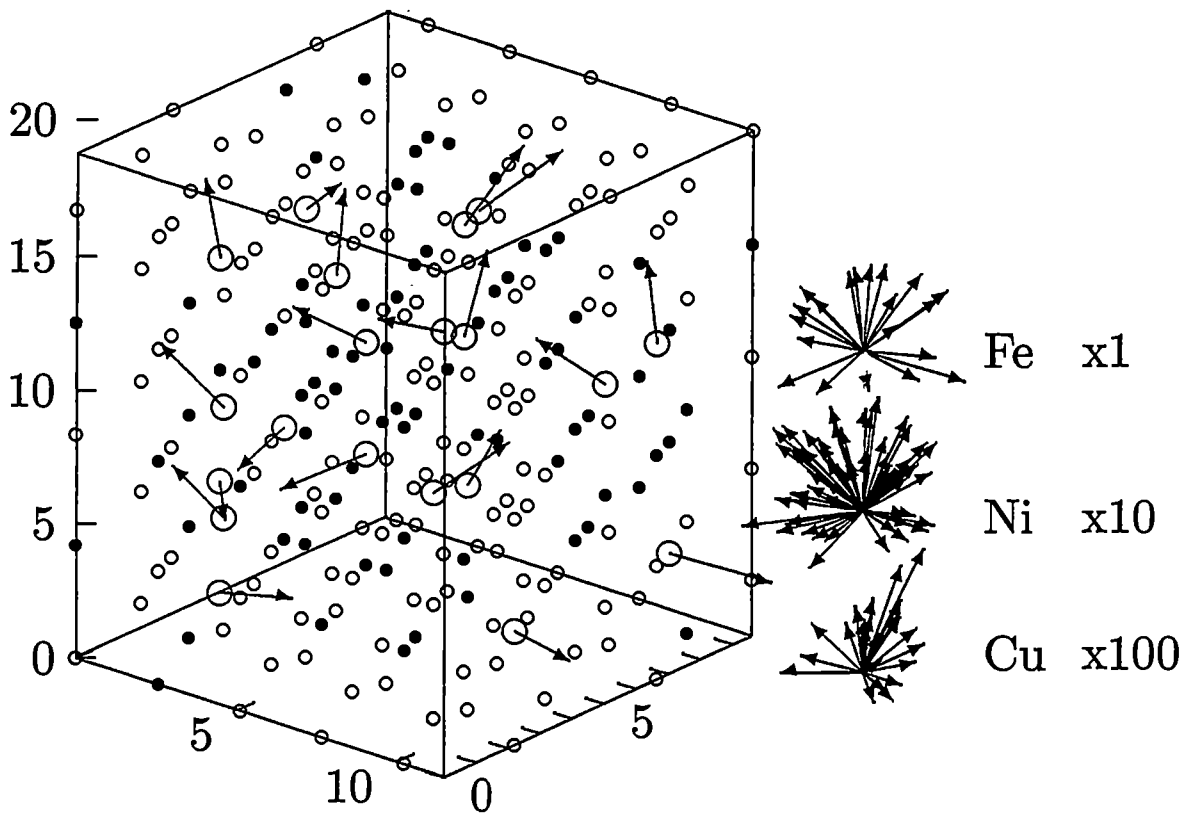

Figure 15: Atomic positions and site magnetic moments for one magnetic configuration of 4 atomic planes of Py interdiffused into Cu. The distances are angstroms and the moments are in Bohr magnetons. The small filled circles represent Ni, the small open circles represent Cu, and the large open circles represent Fe. All Fe moments, as well as, Ni moments greater than $0.15\mu_B$ and Cu moments larger than $0.015\mu_B$ are depicted to the right with the indicated multiplying factors.

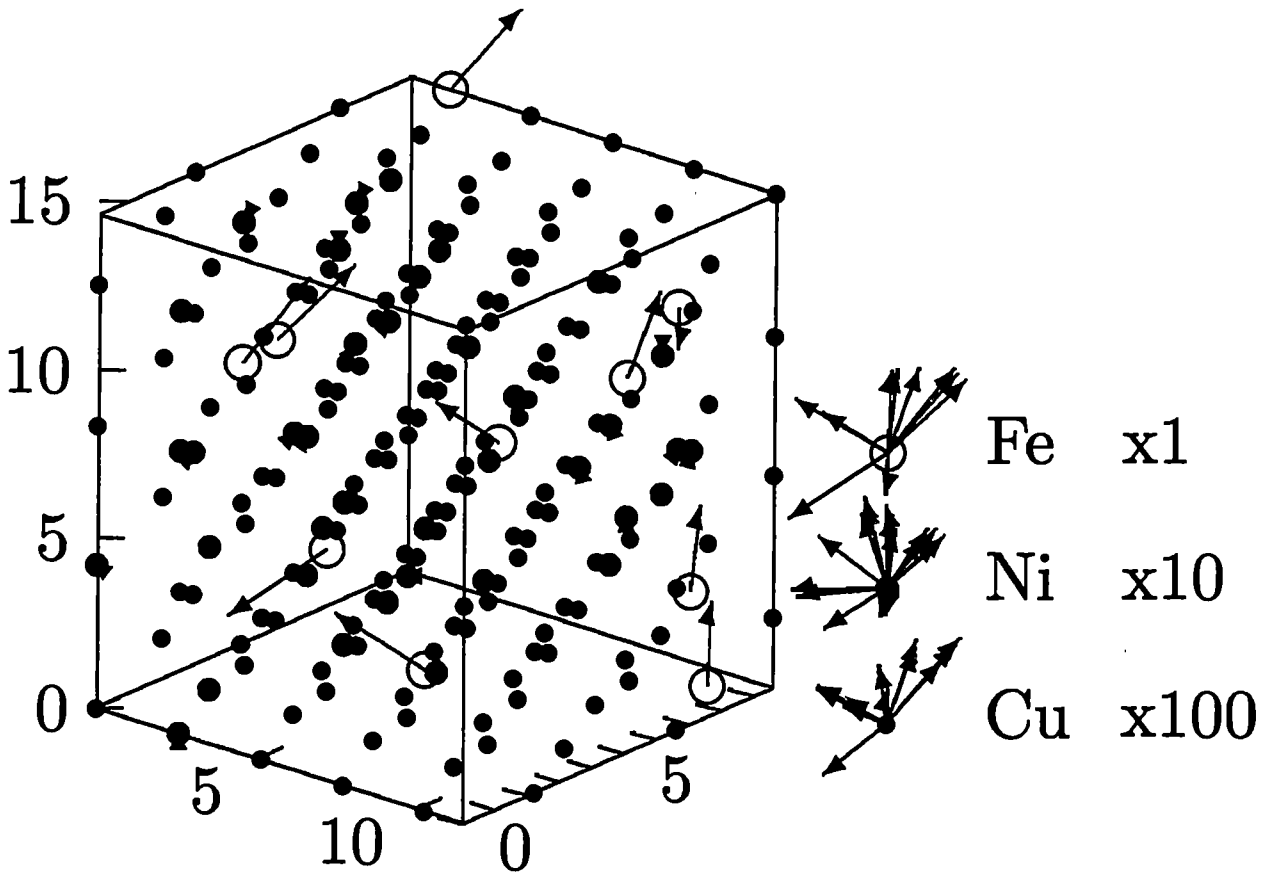

Figure 16: Two layers of permalloy in a copper matrix. The copper and permalloy have been allowed to interdiffuse. Copper atoms are small solid circles, nickel atoms are larger solid circles, iron atoms are large open circles and have large magnetic moments indicated by arrows. The three sets of clasters of arrows to the side of the figure indicate the size of the moments and their directions for the Fe, Ni, and Cu atoms, respectively.

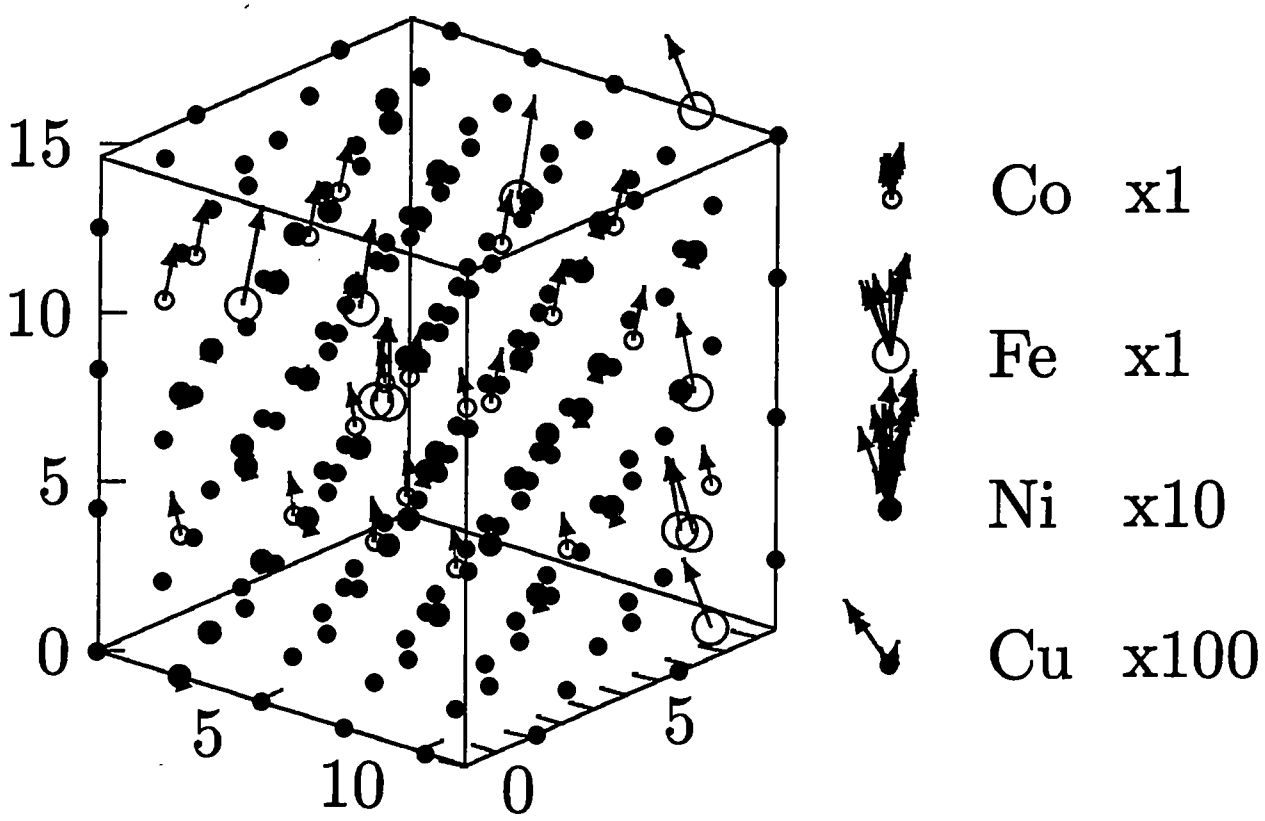

Figure 17: Two layers of permalloy in a copper matrix with cobalt at the interface. In this case cobalt (smaller open circles with arrows) has replaced approximately one half of the copper atoms on the layers above and below the two "permalloy" layers. In both this and the previous figure the layer stacking used in the calculation was hcp (0001) rather than fcc (111). This should have little effect on the calculated moments.

Some of the difficulties that arise when the interfaces interdiffuse are illustrated in Fig. 16 which shows the zero temperature ground state magnetic configuration of two layers of permalloy in a copper matrix after interdiffusion has occurred. The large arrows indicate the Fe moments from the permalloy. These moments are about the same size as in pure permalloy, but their directions have become disordered. These misoriented and "loose" moments will contribute to spin mixing and spin-flip scattering. Furthermore, the nickel moments are much smaller than for pure bulk permalloy so the majority channel does not match nearly so well to copper. When cobalt is added at the interfaces (Fig. 17) the prospects for GMR are improved significantly; the iron moments are in much better alignment and the nickel moments are closer to their bulk values. These calculations were perfomed using the LSMS.

Chapter 6

Conclusions

We have developed the BDA, which is applicable to general atomic arrangements such as ordered intermetallics, substitutionally disorderd alloys, amorphous alloys, layered systems, surfaces etc.. It is an order of magnitude faster than straightforward use of a large LIZ and requires much less memory. With the BDA LIZ sizes as large as a few thousands atoms, depending on the CPU RAM size, can be realized. The ideas in the developing the BDA code helped us accelerate the execution of LSMS code at least 30% speed-up in CPU time.

For the first time it is possible to solve the Kohn-Sham equations for both canted and collinear magnetic arrangements to a high level of convergence. It is found that diffusion at the interface between Py and Cu results in noncollinear magnetic moments. Multiple metastable magnetic configurations for two and four layers of Py in a copper matrix are obtained. The canting of the Fe moments and a reduction of the magnitude of Ni moments at the interface are responsible for the measured "magnetically dead" layers. The calculated noncollinear total spin magnetic moments as a function of the number of Py layers are in good agreement with the experiment.

Also we have discovered that the adding of small amount of Co at the interface can dramatically increase the collinearity. This Co induced increase in collinearity is consistent with improved GMR ratios and observed tolerence greater to the

detrimental effect on GMR ratios of annealing. Calculations of this type appear to provide a very promising tool for design of interfaces. This advantage may, however, be limited because of the presence of multiple metastable magnetic structures. Furthermore, the computing resourses required to perform calculations of this type on the large number of atoms needed to model interfaces will restrict the number of configurations that can be studied.

References

REFERENCES

[1] P. Hohenberg and W. Kohn. *Phys. Rev.* B **136**, 864 (1964).

[2] W. Kohn and L.J. Sham. *Phys. Rev.* **137**, A 1696 (1965).

[3] J.W. Strutt, Baron Rayleigh. *Phil. Mag.* **34**, 4816 (1892).

[4] J. Korringa. *Physica* **13**, 392 (1947).

[5] W. Kohn and N. Rostoker. *Phys. Rev.* **79**, 382 (1950).

[6] P. Soven. *Phys. Rev.* **156**, 809 (1967).

[7] A. Bansil, L. Schwartz, and H. Ehrenreich. *Phys. Rev.* B **12**, 2893 (1975).

[8] G.M. Stocks, B.L. Gyöorffy, E.S Giuliano, and R. Ruggeri. *J. Phys.* F **7**, 1859 (1977).

[9] A.J. Pindor, W.M. Temmerman, B.L. Gyorffy, and G.M. Stocks. *J. Phys.* F **10**, 373 (1970).

[10] H. Winter and G.M. Stocks. *Phys. Rev.* B **27**, 882 (1983).

[11] D.D. Johnson, F.J. Pinski. *Phys. Rev.* B, **48** 1153 (1993).

[12] R. Magri, S.H. Wei, and Alex Zunger. *Phys. Rev.* B, **42** 11388 (1990).

[13] G.M. Stocks, D.M.C. Nicholson, Y. Wang, W.A. Shelton, Z. Szotek, and W.M. Temmerman, in "High Performance Computing symposium; Grand Challenges in Computer Simulation", Proceedings of the 1994 Simulation Multiconference, edited by A.M. Tentner, The Society for Computer Simulation, San Diego, Ca. (1994).

[14] Y. Wang, G.M. Stocks, W.A. Shelton, D.M.C. Nicholson, Z. Szotek, and W.M. Temmerman. *Phys. Rev. Lett.* **75**, 2867 (1995).

[15] P.J. Spencer. *Calphad* **10**, 175 (1986).

[16] M. Ahlers. *Prog. Mater. Sci.* **30**, 135 (1986).

[17] I.A. Abrikosov, A.M.N. Niklasson, S.I. Simak, B. Johansson, A.V. Ruban and H.L. Skriver. *Phys. Rev. Lett.* **76**, 4203 (1996).

[18] I.A. Abrikosov, S.I. Simak, B. Johansson, A.V. Ruban and H.L. Skriver. *Phys. Rev.* B **56**, 9319(1997).

[19] J. Kubler, L.M. Sandratskii, and M. Uhl. *J. Appl. Phys.* **76**, 6694 (1994).

[20] R. Lorenz and J. Hafner. *J. Magn. Magn. Mater.* **139**, 209 (1995).

[21] E. Fawcett. *Rev. Mod. Phys.* **60**, 209 (1988).

[22] A. Herpin, P. Meriel, and J. Villain. *C. R. Acad. Sci.* **249**, 1334(1959).

[23] M. D. Coey. *Can. J. Phys.* **65**, 1210(1987).

[24] R.A. Cowley, N. Cowlam, and L.D. Cussens. *J. Phys. (France) Colloq. C-8* **49**, 1285(1988).

[25] R.A. Cowley, N. Cowlam, P.K. Ivison, and J. Martinez. *J. Magn. Magn. Mater.* **104-107**, 159(1992).

[26] T.J. Hicks and O. Moze. *Philos. Mag.* B **65**, 1191(1992).

[27] Yang Wang, G.M. Stocks, D.M.C. Nicholson, W.A. Shelton, V.P. Antropov and B.N. Harmon. *J. Appl. Phys.* **81**, 3873(1997).

[28] V.S. Speriosu, J.P. Nozieres, B.A. Gurney, B. Dieny, T.C. Huang, and H. Lefakis. *Phys. Rev.* B **47**, 11579(1993).

[29] B.A. Gurney, J.P. Nozieres, V.S. Speriosu, D.R. Wilhoit, and O.U. Need, in Symposium on Magnetic Ultra Thin Films, Multilayers and Surfaces 7, 1992.

[30] J.P. Nozieres, V.S. Speriosu, B.A. Gurney, B. Dieny, H. Lefakis, and T.C. Huang. *J. Magn. Magn. Mater.* **121**, 386(1993).

[31] S.S.P. Larkin. *Phys. Rev. Lett.* **71**, 1641(1993).

[32] D.M.C. Nicholson, W.H. Butler, X.-G. Zhang, J.M. Maclaren, B.A. Gurney and V.S. Speriosu. *J. Appl. Phys.* **76**, 6805(1994).

[33] D.M.C. Nicholson, W.H. Butler, W.A. Shelton, Yang Wang, X.-G. Zhang, G.M. Stocks and J.M. Maclaren. *J. Appl. Phys.* **81**, 4023(1997).

[34] A.B. Oparin, D.M.C. Nicholson, X.-G. Zhang, W.H. Butler, W.A. Shelton, G.M. Stocks and Yang Wang. *J. Appl. Phys.* **85**, 4548(1999).

[35] W.H. Butler, X.-G. Zhang, T.C. Schulthess, D.M.C. Nicholson, A.B. Oparin and J.M. Maclaren. *J. Appl. Phys.* **85**, 5834(1999).

[36] W. Kohn and P. Vashishta, in the chapter "General Density Functional Theory" in "Theory of the Inhomogeneous Electron Gas", edited by S. Lundqvist and N. H. March, Plenum Press, New York, (1983).

[37] B. L. Gyorffy, J. B. Staunton and G. M. Stocks, in "Density Functional Theory", edited by E. K. U. Gross and R. M. Driezler, Plenum Press, New York, 461 (1995).

[38] L.M. Sandratskii. *Advances in Physics,* **47**, 91(1998).

[39] Y. Wang, G. M. Stocks and J. S. Faulkner. *Phys. Rev.* B **49**, 5028 (1994).

[40] U. von Barth and L. Hedin. *J. Phys.* C, **5**, 1629(1972).

[41] D.W. Taylor. *Phys. Rev.* **156**, 1017 (1967).

[42] J.S. Faulkner and G.M. Stocks. *Phys. Rev.* B **21**, 3222 (1980).

[43] B.L. Györffy and M.J. Stott. *Band Structure Spectroscopy of Metals and Alloys,* edited by D.J. Fabian and L.M. Watson (Academic, New York, 1973), p. 385.

[44] J.F. Janak. *Phys. Rev.* B **9**, 3985 (1974).

[45] P.P. Ewald. *Ann. Physik,* **64**, 253 (1921).

[46] G.Y. Guo and W.M. Temmerman. In MRS Symp. Proc. Vol. 253, Applications of Multiple Scattering Theory to Materials Science, p. 317 (1992).

[47] Y. Wang. *Phys. Rev. Lett.* **66**, 1438 (1991).

[48] D.M.C. Nicholson, G.M. Stocks, Y. Wang, W.A. Shelton, Z. Szotek and W.M. Temmerman. *Phys. Rev.* B **50**, 14686 (1994).

[49] J.L. Beeby. *Proc. Roy. Soc. (London),* A **279**, 82 (1964).

[50] A. Gonis, G. M. Stocks, W. H. Butler and H. Winter. *Phys. Rev.* B, **29** 555 (1984).

[51] J.Harris. *Phys. Rev.* B **31**, 1770 (1985).

[52] W.M.C. Foulkes and R.Haydock. *Phys. Rev.* B **31**, 12520 (1985).

[53] M.N. Baibich, J.M. Broto, A. Fert, F. Nguyen Van Dau, F. Petroff, P. Etienne, G. Creuzet, A. Friederich and J. Chaezelas. *Phys. Rev. Lett.* **61**, 2472(1988).

[54] G. Binasch, P. Grünberg, F. Sauerbach and W. Zinn. *Phys. Rev.* B, **39** 4828 (1989).

[55] A. Berkowitz, A.P. Young, J.R. Mitchell, S. Zhang, M.J. Carey, F.E. Spada, F.T. Parker, A. Hutten and G. Tomas. *Phys. Rev. Lett.* **68**, 3745(1992).

[56] J.Q. Xiao, J.S. Jiang and C.L. Chien. *Phys. Rev. Lett.* **68**, 3749(1992).

[57] V.L. Moruzzi and P.M. Marcus. *Phys. Rev.* B, **46** 2864 (1992).

[58] H. Nakotte, K. Prokes, E. Buck, P.F. de Chatel, F.R. de Boer, V. Sechovsky, L. Havela and H. Fujii. *J. Appl. Phys.* **75**, 6522(1994).

[59] W.H. Butler, X.-G. Zhang, D.M.C. Nicholson, and J.M. Maclaren. *J. Magn. Magn. Mater.* **151**, 354 (1995).

[60] S. A. Ahern and W. Sucksmith. *Proc. Phys. Soc.* B, **69**, 1050 (1956).

[61] S. A. Ahern, , M. J. C. Martin, and W. Sucksmith. *Proc. Roy. Soc. (London),* A **248**, 145 (1958).

[62] A. T. Alred, B. D. Rainford, T. J. Hicks, and J. S. Kouvel. *Phys. Rev.* B, **7** 218 (1973).

[63] Y. Wang, G. M. Stocks, D. M. C. Nicholson, and W. A. Shelton. *Alloy Modeling and Design, edited by G.M. Stocks and P.E.A. Turchi(TMS 1994), p. 75.*

[64] D.M.C. Nicholson, W.H. Butler, X.-G. Zhang, J.M. MacLaren, B.A. Gurney and V.A. Speriosu. *J. Appl. Phys.* **76**, 6805(1994).

[65] T.C. Huang, J.P. Nozieres, V.S. Speriosu, B.A. Gurney and H. Lefakis. *Appl. Phys. Lett.* **62**, 1478(1993).

[66] X.W. Zhou and H.N.G. Wadley. *J. Appl. Phys. in press, (1998).*

[67] J.M. MacLaren, S. Crampin, D.D. Vvednsky, R.C. Albers and J.B. Pendry. *Computer Physics Communications,* **60**, 365(1990).

[68] D.M.C. Nicholson and X.A. Zhou. *(unpublished).*

VITA

Andrei Borisovich Oparin was born in Nizhny Novgorod, Russia on October 4, 1962. He attended schools in the central and industrial parts of this city. Almost all his graduation year was spent in the physics and mathematical boarding school at Moscow State University. He graduated from the high school #36 with profound physics and mathematics studying in June, 1979. Two months later he entered Moscow Institute of Physics and Technology. He graduated from this university in June 1985 with Diploma of Engineer-Physicist. After that he had worked as Software Engineer for some institutions and govenrment structures for more than nine years. In August of 1994, he entered Ph.D. program in Physics at The University of Tennessee, Knoxville and became Graduate Research Assistant. Making use of approximity of Oak Ridge National Laboratory to The University of Tennessee, Knoxville, he made his Ph.D. Thesis in Physics with the concentration in Computational First-Principles Condensed Matter Theory. The doctoral degree was received May, 2000.

He is presently looking for job opportunities in computer programming and post-doctoral positions. Also he is considering possibilities to enter a graduate degree program in Computer Science or Engineering.